Aus dem

Institut für Experimentelle und Klinische Pharmakologie und
Pharmakogenomik der Universität Tübingen
Abteilung Pharmakologie, Experimentelle Therapie und
Toxikologie

Effects of $MgCl_2$ and $GdCl_3$ on ORAI1 Expression and Store-Operated Ca^{2+} Entry in Megakaryocytes

Inaugural-Dissertation
zur Erlangung des Doktorgrades
der Medizin

der Medizinischen Fakultät
der Eberhard Karls Universität
zu Tübingen

vorgelegt von

Zhou, Kuo

2022

Dekan: Professor Dr. B. Pichler

1. Berichterstatter   Professor Dr. Dr. B. Nürnberg
2. Berichterstatter: Professor Dr. F. Artunc

Tag der Disputation: 01.12.2022

Table of contents

List of tables

List of figures

List of abbreviations

AGEs	Advanced glycation end products
AM	Acetoxymethyl
ANOVA	Analysis of variance
APS	Ammonium persulfate
β-GP	Beta-glycerophosphate
CAD	CRAC activating domain
CaSR	Ca^{2+}-sensing receptor
CC	Coiled-coil
cDNA	Complementary DNA
CI	Confidence interval
CKD	Chronic kidney disease
CRAC	Ca^{2+} release-activated Ca^{2+}
CT	Cycle threshold
CVD	Cardiovascular disease
DMS	Demarcation membrane system
DMSO	Dimethyl sulfoxide
DNA	Deoxyribonucleic acid
ECL	Enhanced chemiluminescence
eGRF	Estimated glomerular filtration rate
EGTA	Ethylene-glycol-bis(β-aminoethyl)-N,N,N',N'-tetraacetic Acid
ER	Endoplasmic reticulum
ER-PM	Endoplasmic reticulum-plasma membrane
ESRD	End-stage renal disease
FBS	Foetal bovine serum
GAPDH	Glyceraldehyde 3-phosphate dehydrogenase
GPCR	G protein-coupled receptor
GPVI	Glycoprotein VI collagen receptor
HEPES	4-(2-Hydroxyethyl)-piperazine-1-ethanesulfonic acid

HR	Hazard ratio
HRP	Horseradish peroxidase
HSC	Hematopoietic stem cell
IKK	IκB kinase
IS	Indoxyl sulphate
mRNAs	Messenger ribonucleic acids
NFAT5	Nuclear factor of activated T cells 5
NF-κB	Nuclear factor-κB
OASF	ORAI activating small fragment
PBS	Phosphate buffered saline
PCR	Polymerase chain reaction
PDGF	Platelet-derived growth factor
Pi	Inorganic phosphate
PM	Plasma membrane
PMPs	Platelet-derived microparticles
PS	Phosphatidylserine
P/S	Penicillin-Streptomycin
PSGL-1	P-selectin glycoprotein ligand-1
PTH	Parathyroid hormone
PVDF	Polyvinylidene difluoride
qPCR	Quantitative polymerase chain reaction
RIPA	Radioimmunoprecipitation assay
RNA	Ribonucleic acid
ROS	Reactive oxygen species
RPMI	Roswell Park Memorial Institute
SAM	Sterile α-motif
SD	Standard deviation
SDF-1α	Stromal derived factor-1α
SDS	Sodium dodecyl sulphate
SDS-PAGE	Sodium dodecyl sulphate-polyacrylamide gel electrophoresis

SERCA	Sarco/endoplasmic reticulum Ca^{2+}-ATPase
SGK1	Serum and glucocorticoid-inducible kinase 1
SOAR	STIM/ORAI activating region
SOCE	Store-operated Ca^{2+} entry
STIM	Stromal interaction molecule
TBS	Tris buffered saline
TBST	Tris buffered saline, with tween-20
TEMED	N,N,N′,N′-Tetramethylethylenediamine
TGF-β	Transforming growth factor beta
TM	Transmembrane
Tris	Tris-(hydroxymethyl)-aminomethane
VSMCs	Vascular smooth muscle cells

1 Introduction

1.1 Platelet dysfunction in chronic kidney disease

1.1.1 Chronic kidney disease and cardiovascular events

In patients with chronic kidney disease (CKD), cardiovascular disease (CVD) is associated with substantial morbidity and mortality in both developed and developing countries (Edwards et al., 2006, Schiffrin et al., 2007), imposing a tremendous burden on the health care system. The low estimated glomerular filtration rate (eGFR) confers an approximately 3-fold increase in the risk of cardiovascular mortality in patients with end-stage renal disease (ESRD) (Chronic Kidney Disease Prognosis et al., 2010). Even patients with only mild or moderate impaired renal function are at higher risk for subsequent cardiovascular events than the general population is (Anavekar et al., 2004, Mann et al., 2001).

The function of the haemostatic system is profoundly disturbed in patients with renal insufficiency, particularly in patients with ESRD (Ando et al., 2002, Baaten et al., 2021). Accumulating data indicate that these patients have a high prevalence of thrombotic complications, which present as acute coronary syndrome, deep venous thrombosis with/without pulmonary embolism, haemodialysis vascular access thrombosis, as well as peripheral artery occlusion (Lutz and Jurk, 2020, Lutz et al., 2014). Although the imbalance between pro- and anti-coagulant factors (Tomura et al., 1991, Matsuo et al., 1997) and endothelial cell damage (Molino et al., 2006) may help explain excessive thrombus formation, platelet hyperactivity plays a central role in the pathogenesis of thrombosis. Therefore, we mainly discuss the pathogenetic mechanisms underlying platelet dysfunction in the following section.

1.1.2 Mechanisms of platelet dysfunction in renal failure

Multiple mechanisms may be responsible for platelet hyperactivity in patients with CKD (Figure 1).
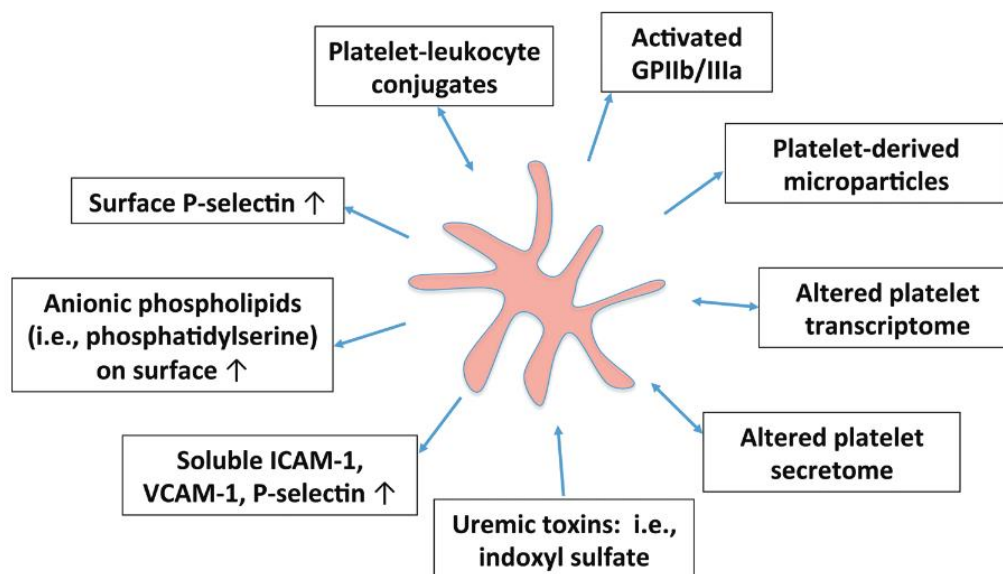
Figure 1. Factors associated with platelet dysfunction in patients with chronic kidney disease (from Lutz and Jurk, 2020).
ICAM-1: intercellular adhesion molecule 1; GP: glycoprotein; VCAM-1: vascular cell adhesion molecule 1.

First, the retention of uraemic toxins, especially indoxyl sulphate (IS), induces platelet hyperactivity in advanced stages of CKD, which contributes to CKD-associated thrombosis (Karbowska et al., 2017, Moradi et al., 2013). Platelet function was found to be remarkably enhanced in a CKD mouse model after IS treatment, which manifested as increased levels of platelet-derived microparticles (PMPs) and platelet-monocyte aggregates in the serum (Yang et al., 2017). IS exhibits a strong ability to promote thrombus formation via reactive oxygen species (ROS)-mediated p38MAPK signalling (Yang et al., 2017), primarily due to the direct impact of oxidative stress in the regulation of platelet activation (Krotz et al., 2004).

In addition, elevated expression of aminophospholipid phosphatidylserine (PS) on the outer surface of platelets obtained from chronic uraemic patients has been described (Bonomini et al., 2007). The thrombophilic tendency of uraemia is partially attributed to PS exposure, which provides a catalytic surface for assembly of the prothrombinase complex that converts prothrombin to thrombin

(Bevers et al., 1991). An increase in caspase-3 activity may be causally linked to this coagulation process (Bonomini et al., 2004).

Furthermore, platelet-leukocyte conjugates are essential for thrombus formation. Physical interactions of activated platelets with leukocytes have been shown to initiate inflammatory and atherogenic cascades at the vascular wall (May et al., 2008, May et al., 2007). A number of studies confirm that circulating platelets under uraemic conditions contain more P-selectin on the surface than those of healthy controls (Sirolli et al., 2001). The engagement of P-selectin glycoprotein ligand-1 (PSGL-1) by P-selectin drives the recruitment of monocytes and neutrophils to the sites of vascular injury, which eventually promotes inflammatory and thrombotic processes (Gawaz et al., 2005, Furie et al., 2001).

1.2 Store-operated Ca^{2+} entry

1.2.1 ORAIs: structure and homologues

Named after the gatekeeper of heaven (Guo and Huang, 2008), ORAI proteins reside in the plasma membrane (PM) and function as the pore-forming subunit of the Ca^{2+} release-activated Ca^{2+} (CRAC) channel that allows Ca^{2+} influx upon stimulation (Hewavitharana et al., 2007, Berna-Erro et al., 2012, Frischauf et al., 2016, Peinelt et al., 2006). Three homologues of the ORAI family were identified in mammals: ORAI1, ORAI2 and ORAI3 (Hoth and Niemeyer, 2013, Motiani et al., 2013). Each ORAI molecule is composed of cytosolic N- and C-termini, as well as four predicted transmembrane (TM) domains that are connected by one intracellular loop and two extracellular loops (Prakriya and Lewis, 2015, Fahrner et al., 2018). A positively charged cluster of amino acids within the TM1 domain exhibits the highest sequence similarity in ORAI family members (Takahashi et al., 2007), whereas non-TM domains are less conserved. The isoform ORAI3 has much longer sequences in the third loop than those of ORAI1 and ORAI2 (Fahrner et al., 2018). Another obvious difference is in the N-

terminus, which contains a proline-/arginine-rich region only in the ORAI1 protein (Frischauf et al., 2011). Among the three ORAI isoforms, the C-terminal putative coiled-coil (CC) domain is critical for channel activation by virtue of its physical interaction with stromal interaction molecule (STIM) 1 (Muik et al., 2008, Frischauf et al., 2009). In contrast, the N-terminal region shows a weaker affinity for STIM1 binding than the C-terminus does, which is likely to regulate STIM1-mediated gating (Lis et al., 2010).

1.2.2 STIMs: structure and homologues

STIMs are single-pass transmembrane proteins comprising of an N-terminal region within the endoplasmic reticulum (ER) lumen and a larger C-terminal portion that faces the cytoplasmic side (Lewis, 2011). Structurally, the luminal part of STIMs is characterized by multiple discrete domains, involving a canonical EF-hand, a hidden EF-hand, a sterile α-motif (SAM), and an α-helical TM domain (Stathopulos et al., 2006, Stathopulos and Ikura, 2010, Schultz et al., 1997). The canonical EF-hand motif, with a typical helix-loop-helix structure, is known to coordinate a single Ca^{2+} ion. The non-canonical motif does not bind Ca^{2+} but facilitates the structural stabilization of the entire EF-SAM entity via hydrogen bonding (Zheng et al., 2011, Stathopulos et al., 2008). The long cytosolic C-terminal strand possesses three CC domains (CC1, CC2, CC3), a serine-/proline-rich region, and a polybasic lysine-rich tail (Fahrner et al., 2017). Moreover, several minimal fragments, such as ORAI-activating small fragment (OASF), CRAC-activating domain (CAD), STIM/ORAI-activating region (SOAR) and Ccb9, have been detected in the C-terminus (Muik et al., 2009, Park et al., 2009, Yuan et al., 2009, Kawasaki et al., 2009), which are adequate to activate CRAC currents in a Ca^{2+} store-dependent manner.

Mammals express two STIM homologues, STIM1 and STIM2 (Soboloff et al., 2012), which share 61% sequence identity (Cahalan, 2009). Differences are

mainly observed in variable regions of the downstream region of the CC2 domain (Ercan et al., 2012, Nguyen et al., 2018). STIM1 is primarily located in the ER, with a limited fraction in the PM (Manji et al., 2000, Luik et al., 2006, Potier and Trebak, 2008), while STIM2 is exclusively localized in the ER due to a strong ER retention sequence at the end of the C-terminal region (Saitoh et al., 2011, Soboloff et al., 2006).

1.2.3 Activation process of store-operated Ca^{2+} entry

Store-operated Ca^{2+} entry (SOCE), which emerged as a ubiquitous mechanism for Ca^{2+} influx (Johnson, 2019), is crucial to sustain a broad spectrum of cellular functions that range from cell proliferation, differentiation and migration to vascular calcification and platelet aggregation (Bootman et al., 2001, Navarro-Borelly et al., 2008). Because of the vital roles of ORAI1 and STIM1 in the regulation of SOCE (Johnstone et al., 2010), we herein focus on the intermolecular steps underlying dynamic STIM1-ORAI1 coupling during SOCE activation.

In the resting state, STIM1 is homogeneously distributed in the bulk ER (Baba et al., 2006). However, upon ER Ca^{2+} store depletion, the dissociation of pre-bound Ca^{2+} from the EF-hand initiates the STIM1 oligomerization process, in which the structural change destabilizes the entire EF-SAM entity and subsequently triggers ER-SAM aggregation (Shim et al., 2015, Stathopulos et al., 2006). The luminal rearrangement further prompts conformational alterations in the TM domain, thus propagating activation signals to the C-terminus (Derler et al., 2016). Following the release of the intramolecular clamp, the undocking of the ORAI-activating domain CAD/SOAR from CC1 allows activated STIM1 to adopt a more extended conformation and migrate towards the ER-plasma membrane (ER-PM) junctions where STIM1 puncta form (Fahrner et al., 2014, Zhou et al., 2013, Luik et al., 2008, Zhang et al., 2005b). In the final step, activated STIM1

multimers recruit ORAI1 to the puncta (Xu et al., 2006). The interaction of STIM1 with ORAI1 enables channel opening and extracellular Ca^{2+} influx into the cytosol (Bhardwaj et al., 2016). A schematic representation linking the depletion of ER Ca^{2+} stores to SOCE activation is depicted in Figure 2.
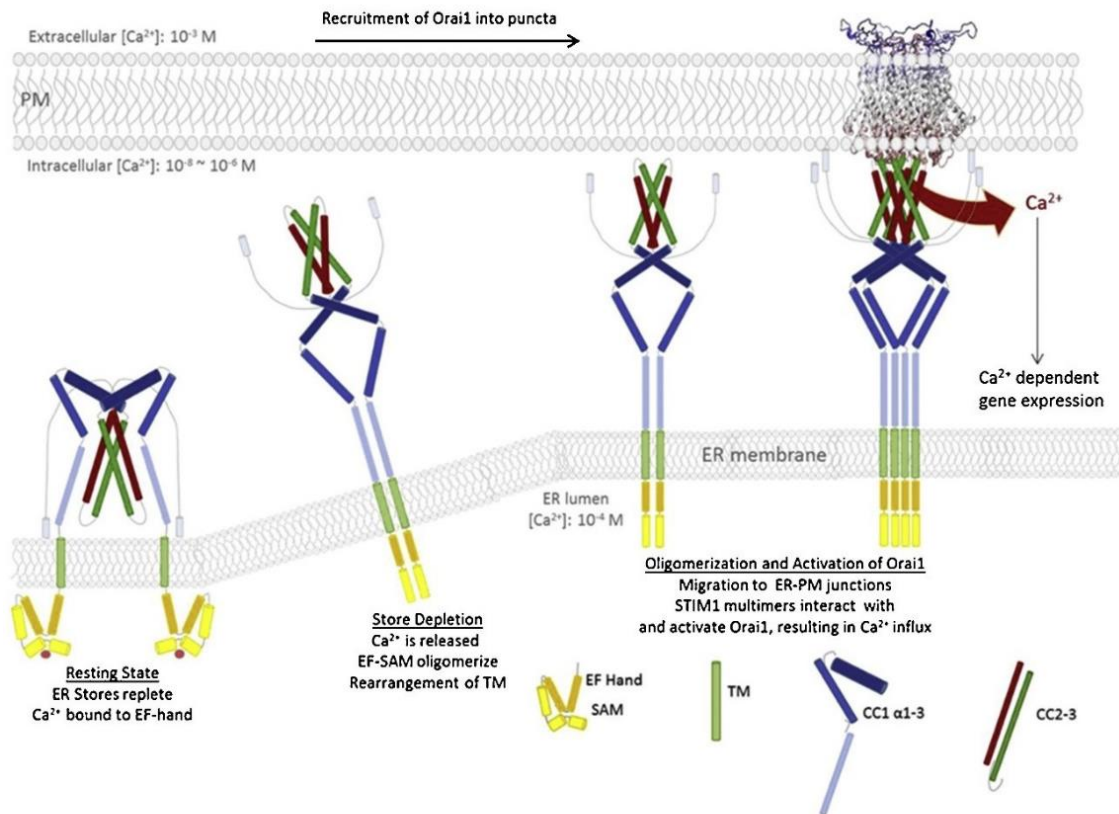
Figure 2. Sequential steps of SOCE activation (from Lunz et al., 2019).
At the resting state, both STIM1 and ORAI1 form homodimers and diffuse evenly in the ER membrane and PM, respectively. Upon a significant drop in ER Ca^{2+} concentration, Ca^{2+}-disassociation from the EF-hand triggers STIM1 oligomerization, followed by the migration of STIM1 oligomers to ER-PM junctions. After ORAI1 recruitment, the undocking of the SOAR domain from CC1 allows the interaction between activated STIM1 and the ORAI1 protein, and thus causes Ca^{2+} influx. CC1: coiled-coil domain 1; CC2-3: coiled-coil domain 2-3; ER: endoplasmic reticulum; PM: plasma membrane; SAM: sterile α-motif; TM: transmembrane.

1.2.4 Regulation of platelet function by ORAI1/STIM1

At sites of vascular injury, platelet adhesion, degranulation, activation and

aggregation are essential to limit blood loss, but may also lead to ischaemia or infarction of vital organs (Nieswandt and Watson, 2003). The central event of platelet activation is an agonist-induced increase in intracellular Ca^{2+} concentration ($[Ca^{2+}]_i$) (Berna-Erro et al., 2016), which occurs via Ca^{2+} release from internal stores and extracellular Ca^{2+} influx (Varga-Szabo et al., 2011, Braun et al., 2011). In human platelets, the Ca^{2+} influx pathway primarily depends on SOCE, which is accomplished by two major determinants, ORAI1 and STIM1 (Lang et al., 2013).

Bergmeier et al. observed that platelets expressing an inactive form of ORAI1 ($ORAI1^{R93W}$) had a marked reduction in SOCE and a defect in agonist-induced Ca^{2+} responses. Moreover, $ORAI1^{R93W}$ platelets were associated with blunted integrin activation and reduced degranulation when stimulated by low concentrations of agonist (Bergmeier et al., 2009). Varga-Szabo et al. reported that, in addition to defective store-operated Ca^{2+} influx, integrin activation and thrombi growth were dramatically impaired in $Stim1^{-/-}$ platelets under conditions of high shear stress (Varga-Szabo et al., 2008). Overall, these results establish ORAI1 and its regulator STIM1 as important mediators of thrombin generation in ischaemic cardiovascular events.

1.3 Ca^{2+} signalling in megakaryocytes

1.3.1 Megakaryocyte development and platelet formation

Since platelets are anucleate cell fragments derived from megakaryocytes (Garraud and Cognasse, 2015), they only contain post-transcriptional mechanisms to regulate specific protein expression, due to the lack of genomic deoxyribonucleic acid (DNA) (Nassa et al., 2018). At the final stage of differentiation, megakaryocytes release platelets by converting their cytoplasm into tubelike extensions (Golfier et al., 2010). As a result, platelets inherit megakaryocyte cytoplasm, especially the messenger ribonucleic acids (mRNAs)

and proteins in the cytoplasm (Garraud and Cognasse, 2015) which play key roles in the following platelet activation. Therefore, we place particular emphasis on the process of thrombopoiesis, by which mature megakaryocytes originate from haematopoietic stem cells (HSCs) and produce platelets (Kaushansky, 2015, Woolthuis and Park, 2016).

Megakaryocytes have large nuclei (50–100 μm) and account for only 0.01% of nucleated bone marrow cells (Machlus and Italiano, 2013). Nevertheless, a single megakaryocyte can generate up to 10^4 platelets during its lifespan (Kaufman et al., 1965, Patel et al., 2005). The first phase of megakaryocyte development generally takes a few days to complete. Early in ontogeny, megakaryocytes increase their DNA content by initiating endomitosis to form polyploid multilobed nuclei (Di Buduo et al., 2016). To assemble platelets, an expansion of the megakaryocyte cytoplasm occurs, followed by the accumulation of distinctive components, including cytoskeletal proteins, platelet-specific secretory granules and the demarcation membrane system (DMS) (Italiano and Shivdasani, 2003). During the second stage, megakaryocytes get in close proximity to bone marrow sinusoids under the chemoattraction of stromal-derived factor-1α (SDF-1α) (Hamada et al., 1998). Then, by remodelling their cytoskeletal structures, megakaryocytes extend multiple long pseudopods (pro-platelets) into the lumen of sinusoidal blood vessels, where they undergo subsequent fission events to release platelets (Figure 3A) (Italiano et al., 1999). This phase is rapidly completed within hours.

1.3.2 ORAI1/STIM1-dependent Ca^{2+} signalling in megakaryocytes

Our previous observations revealed that the transcription factor nuclear factor of activated T cells 5 (NFAT5) is a powerful stimulator of SOCE into megakaryocytes via serum and glucocorticoid-inducible kinase 1 (SGK1)-dependent upregulation of ORAI1 expression (Figure 3B).

The NFAT5 expression level and activity are enhanced in several clinical disorders, such as inflammation, diabetes mellitus, dehydration and hyperphosphatemia of CKD (Hernandez-Ochoa et al., 2012, Neuhofer, 2010, Leibrock et al., 2015). Genes upregulated by NFAT5 include SGK1, a potent regulator of ORAI1 (Sahu et al., 2017). Genetic knockout or pharmacological inhibition of SGK1 contributes to lower ORAI1 abundance, impaired integrin activation, as well as a decrease in collagen-triggered thrombus formation (Eylenstein et al., 2011, Borst et al., 2012). SGK1 has recently been shown to phosphorylate IκB kinase alpha/beta (IKKα/β), which phosphorylates the nuclear factor-κB (NF-κB) inhibitory protein IκB, leading to the degradation of IκB and subsequent translocation of the NF-κB p65 subunit to the nucleus (Lang et al., 2015, Zhang et al., 2005a). In addition, NF-κB triggers the transcription of ORAI1 and the Ca^{2+} sensor SITM1. The opening of the ORAI1 channel by STIM1 results in SOCE, and thus controls megakaryocyte differentiation, migration and platelet production via the regulation of cytosolic Ca^{2+} activity (Sahu et al., 2017).
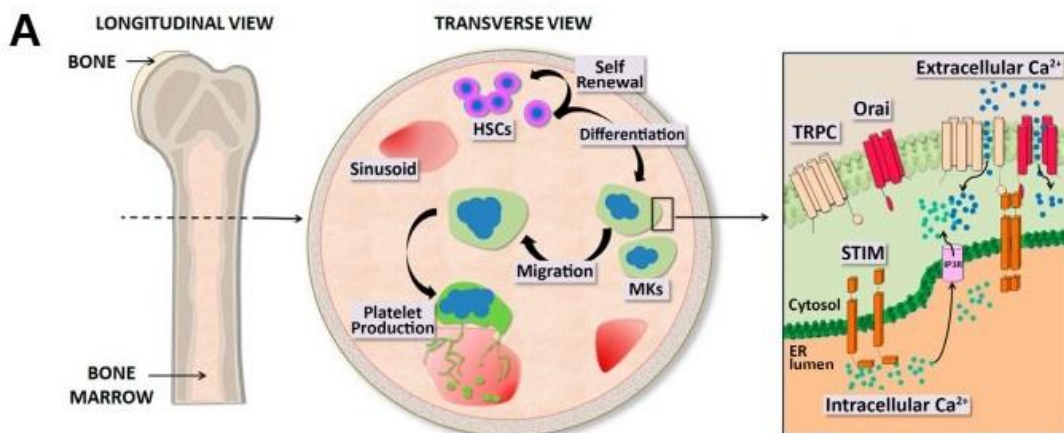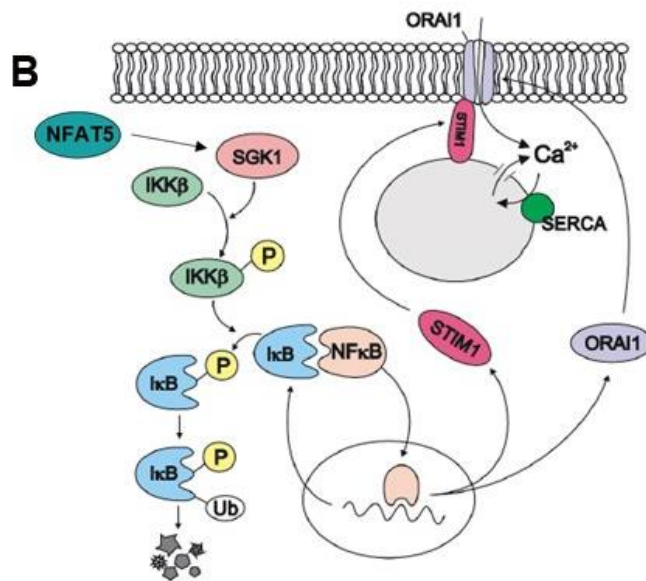
Figure 3. The function and regulation of SOCE in physiological thrombopoiesis.
(A). SOCE finely regulates physiological megakaryocyte functions (adapted from Di Buduo et al., 2016). During physiological thrombopoiesis, HSCs commit and differentiate toward megakaryocytes under the stimulation of thrombopoietin. In megakaryocytes with replete ER, STIM adopts an inactive configuration on the ER membrane. The depletion of ER Ca^{2+} store initiates the STIM oligomerization and subsequent translocation to the plasma membrane. Following ORAI recruitment, the interaction between STIM and ORAI results in the opening of SOCE, which in turn controls megakaryocyte differentiation, migration and final platelet production through the regulation of cytosolic Ca^{2+} concentration. **(B).** Regulation of ORAI1/STIM1 by NFAT5 and SGK1 in megakaryocytes (adapted from Lang et al., 2013). In megakaryocytes, genes upregulated by NFAT5 include SGK1. SGK1 phosphorylates IKKβ, which in turn phosphorylates and inactivates IκB, the inhibitor of NF-κB. The release of NF-κB from NF-κB-IκB complex permits the nuclear translocation of subunit p65 and the induction of ORAI1 and STIM1 transcription. HSC: hematopoietic stem cell; IKKβ: IκB kinase beta; MKs: megakaryocytes; NFAT5: nuclear factor of activated T cells 5; NF-κB: nuclear factor-κB; SERCA: sarco/endoplasmic reticulum Ca^{2+}-ATPase; SGK1: serum and glucocorticoid-inducible kinase 1; STIM1: stromal interaction molecule1; TRPC: transient receptor potential canonical.

1.3.3 Effect of phosphate on Ca^{2+} signalling

Renal phosphate excretion is the principal mechanism for the maintenance of phosphate homeostasis (Hruska et al., 2008). Compromised renal elimination results in a positive phosphate balance in CKD, with a subsequent increase in

phosphate concentrations in plasma and diverse tissues. As CKD progresses, hyperphosphatemia accelerates vascular calcification and atrial stiffness, which in turn lead to cardiovascular events and a high risk for all-cause mortality (Blacher et al., 2001, Mizobuchi et al., 2009).

In vascular smooth muscle cells (VSMCs), elevated extracellular phosphate induces ORAI1/STIM1 expression and SOCE, which participates in the orchestration of osteo/chondrogenic transdifferentiation and vascular calcification (Ma et al., 2019). Similar results were observed in the same lab. Platelets from patients with impaired renal function showed higher transcript levels of *NFAT5*, *SGK1*, *ORAI* and *STIM* isoforms than those of platelets isolated from healthy subjects. Moreover, the phosphate-donor β-glycerophosphate has been reported to upregulate SOCE in megakaryocytes, an effect mediated by activation of the signalling cascade involving NFAT5, SGK1, ORAI1/2/3, and STIM1/2 (Pelzl et al., 2020).

1.4 Effect of Mg^{2+}

1.4.1 Role of Mg^{2+} in CKD

Mg^{2+}, a major intracellular cation, serves as an important cofactor for enzyme systems and transporters that are essential for many biological processes (Swaminathan, 2003, Vormann, 2003). Normal Mg^{2+} levels in human serum range from 0.76 mM to 1.15 mM (Grober et al., 2015). In CKD, the occurrence of hypomagnesemia is commonly observed due to inadequate dietary Mg^{2+} intake and the use of diuretics or medications such as antibiotics like tetracyclines that inhibit Mg^{2+} absorption. The use of large amounts of low-Mg^{2+} dialysate or Mg^{2+}-free dialysate in patients receiving dialysis may be another potential reason for the obvious decline in serum Mg^{2+} concentration (Varghese et al., 2020, Seo and Park, 2008).

Mg^{2+} deficiency predisposes patients to atherosclerosis and arterial

calcification, both of which are considered as strong predictors of cardiovascular mortality in CKD (Xiong et al., 2019, Massy and Drueke, 2012). Several studies have documented that dietary Mg^{2+} supplementation prevents the development of vascular calcification in different animal models of CKD (Kaesler et al., 2020, Zelt et al., 2015). A meta-analysis of 22 longitudinal studies revealed that each 0.1 mM increment in Mg^{2+} exposure was associated with a reduced overall risk for cardiovascular mortality or events [hazard ratio (HR): 0.85; 95% confidence intervals (CI): 0.77-0.94; $p < 0.001$] and all-cause mortality (HR: 0.90; 95% CI: 0.87-0.94; $p < 0.001$) in patients with CKD (Leenders et al., 2021). In addition, Mg^{2+}-based interventions exert beneficial impacts on surrogate markers of cardiovascular outcomes under CKD conditions, such as carotid intima-media thickness and serum calcification propensity, and these results have been validated in multiple randomized controlled clinical trials (Mortazavi et al., 2013, Bressendorff et al., 2017, Bressendorff et al., 2018). It is, therefore, reasonable to speculate that Mg^{2+} supplementation confers an improved clinical prognosis for CKD patients.

1.4.2 Mg^{2+} and Ca^{2+}-sensing receptor

Ca^{2+}-sensing receptors (CaSRs) are unique members of the G protein-coupled receptor (GPCR) superfamily (Conigrave and Ward, 2013), and these receptors act as important master controllers of the Ca^{2+} homeostatic system by modulating the secretion of parathyroid hormone (PTH), the synthesis of active vitamin D, as well as the absorption and resorption of Ca^{2+} in response to changes in serum Ca^{2+} levels (Coburn et al., 1999). Existing evidence suggests that CaSRs are highly expressed in key tissues that participate in extracellular Ca^{2+} homeostasis, such as the parathyroid gland, kidney, intestine and bone, where its physiological roles have not been fully characterized (Riccardi et al., 1995, Chang et al., 1999, Chattopadhyay et al., 1998). CaSR expression is also

observed in many other tissues, where it is indirectly involved in Ca^{2+} homeostasis, such as the brain, breast, airway, liver and arteries. However, the function of CaSRs in these tissues is so far undefined (Diaz-Soto et al., 2016).

Although extracellular Ca^{2+} is the primary ligand of CaSRs with high cooperativity, CaSRs also bind to diverse endogenous stimuli, including inorganic divalent or trivalent cations (e.g., Mg^{2+}, Gd^{3+}, Ba^{2+}, and Al^{3+}) and basic polypeptides (Gerbino and Colella, 2018, Brennan et al., 2013). In parathyroid cells, Mg^{2+} has been previously demonstrated to reduce PTH release via the upregulation of CaSRs (Rodriguez-Ortiz et al., 2014). Similarly, CaSR activation by Mg^{2+} interferes with osteo/chondrogenic signalling and counteracts calcification in VSMCs, and another CaSR orthosteric agonist, Gd^{3+}, mimicked this effect (Alesutan et al., 2017). The stimulation of osteo/chondrogenic signalling by phosphate requires ORAI1 (Ma et al., 2019). Recent observations indicated that Mg^{2+} and Gd^{3+} favourably influence phosphate-induced vascular calcification by inhibiting the upregulation of ORAI1 and STIM1, as well as the suppression of SOCE (Zhu et al., 2020).

The presence of CaSRs has been previously evidenced in both platelets and megakaryocytes (House et al., 1997), and CaSR activation has been proposed to counteract platelet aggregation in hyperhomocysteinemia (Wang et al., 2017b). Nevertheless, to the best of our knowledge, whether Mg^{2+} and the CaSR agonist Gd^{3+} reverse the stimulatory effect of phosphate on ORAI1 and STIM1 expression and SOCE activity in megakaryocytes has not been elucidated.

1.5 Aim of the present study

The present study was designed to investigate whether Mg^{2+} or Gd^{3+} modifies the transcript levels of *NFAT5*, *SGK1*, *ORAI1*, *ORAI 2*, *ORAI 3*, *STIM1*, *STIM2* and the protein levels of ORAI1 and STIM1, and SOCE in megakaryocytes in the absence and presence of prior incubation with the phosphate donor β-glycerophosphate.

2 Materials and methods

2.1 Materials

2.1.1 Chemicals and reagents

Table 1. List of chemicals and reagents in the study

Name	Catalog number	Manufacturer
Acrylamide/Bis-solution 30 (29:1)	A124.2	Carl Roth
Ammonium persulfate (APS)	A3678-25G	Sigma-Aldrich
Aqua clean	WAK-AQ-250-50L	WAK-Chemie Medical GmbH
β-Glycerophosphate disodium salt hydrate	G9422-100G	Sigma-Aldrich
Bio-Rad protein assay dye reagent concentrate	500-0006	Bio-Rad Laboratories
$CaCl_2 \cdot 2H_2O$	C3881-500G	Sigma-Aldrich
Chloroform	6340.2	Carl Roth
Developer solution	RP X-OMAT Developer	Carestream Health
D-(+)-glucose	G7528-1KG	Sigma-Aldrich
Dimethyl sulfoxide (DMSO)	A994.1	Carl Roth
Disinfection	00-311-010	Dr. Schumacher GmbH
Dulbecco's phosphate buffered saline (PBS)	D8537-500ML	Sigma-Aldrich
Ethanol	20821.330	VWR International
Ethylene-glycol-bis(β-aminoethyl)-N,N,N',N'-tetraacetic acid (EGTA)	325626	CalbioChem GmbH
Foetal bovine serum (FBS)	10270-106	Gibco Life Technologies
Fixer solution	RP X-OMAT LO	Carestream Health

	Fixer	
Fura-2, acetoxymethyl (AM)	F1221	Invitrogen
GdCl$_3$	439770-5G	Sigma-Aldrich
Glycine	3908.3	Carl Roth
GoScript™ reverse transcription kit	A5001	Promega
GoTaq® qPCR Master Mix	A6002	Promega
HCl	0281.1	Carl Roth
4-(2-Hydroxyethyl)-piperazine-1-ethanesulfonic acid (HEPES)	HN78.2	Carl Roth
Isopropanol	AE73.1	Carl Roth
KCl	6781.1	Carl Roth
Methanol	34860-2.5L-R	Sigma-Aldrich
MgCl$_2$	M8266-1KG	Sigma-Aldrich
MgSO$_4$ • 7H$_2$O	A6287,1000	AppliChem GmbH
NaCl	S7653-1KG	Sigma-Aldrich
Na$_2$HPO$_4$	A2943,1000	AppliChem GmbH
NaOH	S8045-500G	Sigma-Aldrich
N,N,N′,N′-Tetramethylethylenediamine (TEMED)	2367.3	Carl Roth
Nuclease-free water	P119E	Promega
PageRuler™ pre-stained protein ladder (10 to 180 kDa)	26616	Thermo Fisher Scientific
Penicillin-Streptomycin (P/S)	P0781-100ML	Sigma-Aldrich
PeqGOLD TriFast™	30-2010	VWR International
Pierce™ enhanced chemiluminescence (ECL) Western blotting substrate	32106	Thermo Fisher Scientific
Poly-L-lysine solution (0.01%)	P4704-50ML	Sigma-Aldrich
Powdered milk	T145.3	Carl Roth

Protease inhibitor cocktail (100x)	87786	Thermo Fisher Scientific
Protein gel loading buffer (4x)	K929.1	Carl Roth
Radioimmunoprecipitation assay (RIPA) buffer (10x)	9806S	Cell Signalling Technology
Roswell Park Memorial Institute medium (RPMI) 1640 medium, GlutaMAX™ supplement	61870-010	Gibco Life Technologies
Silicone paste	5874.3	Carl Roth
Sodium dodecyl sulphate (SDS)	0183.3	Carl Roth
Thapsigargin	T7458	Invitrogen
Tris-(hydroxymethyl)-aminomethane (Tris)	4855.2	Carl Roth
Trypan blue solution (0.4%)	15250061	Gibco Life Technologies
Tween-20	9127.1	Carl Roth
Water	W3500-1L	Sigma-Aldrich

2.1.2 Buffers, solutions and culture media

Table 2. List of buffers, solutions and culture media in the study

Buffers/Solutions/Culture media	Composition	
10% APS	APS	1 g
	ddH_2O	10 mL
10% SDS	SDS	5 g
	ddH_2O	50 mL
1.5 M Tris-HCl	Tris	1.5 M (36.33 g)
	ddH_2O	200 mL
	pH	8.8
1.0 M Tris-HCl	Tris	1.0 M (24.22 g)
	ddH_2O	200 mL

	pH	6.8
Sodium dodecyl sulphate-polyacrylamide gel electrophoresis (SDS-PAGE) running buffer (10x)	Tris	250 mM (30.3 g)
	Glycine	1.92 M (144 g)
	SDS	1% (10 g)
	ddH$_2$O	1 L
	pH	8.3
SDS-PAGE running buffer (1x)	SDS-PAGE running buffer (10x)	10% (100 mL)
	ddH$_2$O	900 mL
Transfer buffer (10x)	Tris	250 mM (30.3 g)
	Glycine	1.92 M (144 g)
	ddH$_2$O	1 L
Transfer buffer (1x)	Transfer buffer (10x)	10% (100 mL)
	Methanol	20% (200 mL)
	ddH$_2$O	700 mL
Tris buffered saline (TBS) (10x)	Tris	200 mM (24.2 g)
	NaCl	1.37 M (80 g)
	ddH$_2$O	1 L
	pH	7.6
Tris buffered saline, with tween-20 (TBST) (0.1%)	TBS (10x)	10% (100 mL)
	Tween-20	0.1% (1 mL)
	ddH$_2$O	900 mL
Standard HEPES solution	NaCl	125 mM (3.653 g)
	KCl	5 mM (0.1864 g)
	MgSO$_4$ • 7H$_2$O	1.2 mM (0.15 g)
	HEPES	32 mM (3.84 g)
	Na$_2$HPO$_4$	2 mM (0.142 g)
	Glucose	5 mM (0.45 g)
	CaCl$_2$ • 2H$_2$O	1 mM (0.074 g)
	ddH$_2$O	500 mL
	pH	7.4

Ca^{2+}-free HEPES solution	NaCl	125 mM (3.653 g)
	KCl	5 mM (0.1864 g)
	MgSO$_4$ • 7H$_2$O	1.2 mM (0.15 g)
	HEPES	32 mM (3.84 g)
	Na$_2$HPO$_4$	2 mM (0.142 g)
	Glucose	5 mM (0.45 g)
	EGTA	0.5 mM (0.095 g)
	ddH$_2$O	500 mL
	pH	7.4
75% Ethanol	Ethanol	75% (30mL)
	Nuclease-free water	25% (10mL)
RPMI 1640 culture medium	RPMI 1640 medium	89% (445 mL)
	FBS	10% (50 mL)
	P/S	1% (5 mL)

2.1.3 Antibodies

Table 3. List of the used antibodies

Name	Catalog number	Manufacturer
Anti-GAPDH antibody	2118S	Cell Signalling Technology
Anti-ORAI1 antibody	13130-1-AP	Proteintech
Anti-rabbit horseradish peroxidase (HRP)-conjugated antibody	7074S	Cell Signalling Technology
Anti-STIM1 antibody	4916S	Cell Signalling Technology

2.1.4 Consumables

Table 4. List of the used disposables

Name	Type	Catalog number	Manufacturer

Adhesive sealing films	50 pcs	732-3228	VWR International
Amersham hyperfilm ECL	18×24 cm	28906837	GE healthcare
Cell culture dishes	35×10 mm	627160	Greiner Bio-One GmbH
Cell culture flasks	T-25	83.3910.002	Sarstedt AG
Cell culture flasks	T-75	83.3911.002	Sarstedt AG
Cell culture plates	6-well	353046	Corning Inc.
Cell culture plates	12-well	351143	Corning Inc.
Centrifuge tubes	15 mL	188271	Greiner Bio-One GmbH
Centrifuge tubes	50 mL	227261	Greiner Bio-One GmbH
Cover glasses	30 mm	631-0174	VWR International
Cryogenic vials	1.2 mL	430487	Corning Inc.
Filter tips	0.1-10 µL	81-1010	VWR International
Filter tips	1-20 µL	S1123-1810	STARLAB GmbH
Filter tips	1-100 µL	701061	Biozym Scientific GmbH
Filter tips	1-200 µL	S1120-8810	STARLAB GmbH
Filter tips	100-1000 µL	81-1050	VWR International
Immun-Blot polyvinylidene difluoride (PVDF) membranes	0.2 µm	1620177	Bio-Rad Laboratories
Pipette tips	0.1-10 µL	P866.1	Carl Roth
Pipette tips	1-200 µL	E707.1	Carl Roth
Pipette tips	100-1000 µL	686290	Greiner Bio-One GmbH
qPCR plates	96-well	732-2386	VWR International
Reaction tubes	200 µL	72.737.002	Sarstedt AG
Reaction tubes	500 µL	0030124537	Eppendorf AG
Reaction tubes	1.5 mL	616201	Greiner Bio-One GmbH
Semi-micro cuvette	330 nm	67.742	Sarstedt AG
Serological pipettes	2 mL	4021	Corning Inc.

Serological pipettes	5 mL	4051	Corning Inc.
Serological pipettes	10 mL	4101	Corning Inc.
Serological pipettes	25 mL	4251	Corning Inc.
UVette®	220-1600 nm	0030106.300	Eppendorf AG
Western blotting filter papers	7×8.4 cm	1703966	Bio-Rad Laboratories

2.1.5 Equipment

Table 5. List of the instruments used in the study

Name	Manufacturer
Axiovert 100 inverted fluorescence microscope	Zeiss, Oberkochen, Germany
Bio-photometer plus	Eppendorf AG, Hamburg, Germany
Block thermostat	Carl Roth, Karlsruhe, Germany
Camera control panel	Proxitronic, Bensheim, Germany
Centrifuge	Andreas Hettich GmbH, Tuttlingen, Germany
Centrifuge	Eppendorf AG, Hamburg, Germany
Centrifuge	Thermo Fisher Scientific, Langenselbold, Germany
CFX Connect™ real-time polymerase chain reaction (PCR) detection system	Bio-Rad Laboratories, Hercules, CA, USA
Clean bench	Thermo Electron LED GmbH, Langenselbold, Germany
Drying oven	Memmert GmbH, Schwabach, Germany
Filter wheel changer	Sutter Instrument Company, Novato, CA, USA
Freezer (-20°C)	Liebherr International AG, Bulle, Switzerland
Freezer (-80°C)	Forma Scientific Inc., Marietta, GA, USA
Fridge (+4°C)	Liebherr International AG, Bulle, Switzerland
Heraeus incubator	Thermo Fisher Scientific, Waltham, MA, USA

Mini trans-blot electrophoretic transfer cell	Bio-Rad Laboratories, Hercules, CA, USA
Objective fluor 40×/1.30 oil immersion	Zeiss, Oberkochen, Germany
pH meter	SI Analytics GmbH, Mainz, Germany
Platform shaker	Heidolph Instruments GmbH, Schwabach, Germany
Precision scale	Kern & Sohn GmbH, Balingen, Germany
Precision scale	Denver Instrument GmbH, Göttingen, Germany
Roller mixer	Phoenix Instrument GmbH, Garbsen, Germany
Roller mixer	Stuart Equipment, Staffordshire, United Kingdom
Scanner	Epson, Nagano, Japan
Thermal cycler	Eppendorf AG, Hamburg, Germany
Thermal printer	Seiko Instruments Inc., Chiba-shi, Japan
Vortex mixer	Scientific Industries Inc., New York, NY, USA
Water bath	Julabo GmbH, Seelbach, Germany
Xenon lamp XBO 75W/2	Leistungselektronik Jena GmbH, Jena, Germany

2.1.6 Software

Table 6. List of the used software

Software	Version	Manufacturer
CFX Manager^{TM} software	3.1	Bio-Rad Laboratories
EndNote	20	Clarivate
GraphPad Prism	8.0	GraphPad Software
ImageJ	1.52	National Institutes of Health
MetaFluor	7.5	Universal Imaging Corporation
Photoshop	CS4	Adobe Systems
SPSS	25.0	SPSS Inc.
Word/Excel/PowerPoint	2010	Microsoft

2.2 Methods

2.2.1 Cell culture

2.2.1.1 Used cell line

The human megakaryoblastic cell line Meg-01 used in the current study was acquired from American Type Culture Collection (ATCC, Manassas, VA, USA). Meg-01 cells display similar phenotypic properties to those of normal human megakaryocytes (Takeuchi et al., 1998, Ogura et al., 1985), thus allowing the cell line to be widely used as an *in vitro* model for studying the mechanisms regulating SOCE in thrombopoiesis.

2.2.1.2 Cultivation of Meg-01 cells

Meg-01 cells were cultured in RPMI 1640 medium containing GlutaMAX, routinely supplemented with 10% FBS (Gibco, Paisley, United Kingdom) and 1% P/S (Sigma-Aldrich, Steinheim, Germany). All of the cells were maintained in ventilated culture flasks, stored at 37ºC in a humidified 5% CO_2 incubator and passaged every three or four days. To avoid contamination, the culture procedures were performed under sterile conditions inside a laminar flow hood.

2.2.1.3 Cryopreservation of cells

After washing and centrifugation, the cell pellet was resuspended in cell-freezing medium comprising 70% RPMI 1640 medium, 20% FBS and 10% DMSO (Carl Roth, Karlsruhe, Germany). One millilitre of the cell suspension was aliquoted into each cryovial, which was kept at 4°C for 10 min, -20°C for 30 min and -80°C overnight, and then transferred to the vapour phase of liquid nitrogen at -196°C for long-term storage.

2.2.1.4 Cells thawing

For re-cultivation, the cryovial was removed from the liquid nitrogen tank and quickly thawed at 37°C. To remove DMSO, cells were diluted with pre-heated RPMI 1640 medium containing 10% FBS and centrifuged at 300 g for 5 min. The

supernatant was discarded before the pellet was resuspended in 5 mL of cell culture medium. Thereafter, the cell suspension was transferred to a new culture flask filled with the culture medium to a final volume of 15 mL.

2.2.2 Quantitative polymerase chain reaction (qPCR)

To detect the relative transcription levels of *CaSR*, *NFAT5*, *SGK1*, *ORAI1*, *ORAI2*, *ORAI3*, *STIM1* and *STIM2*, real-time qPCR was employed. Megakaryocytes were harvested in peqGOLD TriFast™ reagent (Peqlab, Erlangen, Germany), and total ribonucleic acid (RNA) extraction was conducted according to the manufacturer's protocols. Following DNase digestion, 5 µg of total RNA was reverse transcribed to generate complementary DNA (cDNA) using the GoScript™ reverse transcription system (Promega, Mannheim, Germany) with Oligo(dT)$_{15}$ primers (Promega, Mannheim, Germany). In the next step, PCR amplification and real-time fluorescence monitoring were carried out using CFX96 real-time detection system (Bio-Rad Laboratories, Munich, Germany). All reactions were performed in duplicate with a final volume of 15 µL, which contained 100 ng of template cDNA, 500 nM forward primer, 500 nM reverse primer and 7.5 µL 2x GoTaq® qPCR Master Mix buffer (Promega, Hilden, Germany). The thermal cycling conditions applied for amplification involved an initial 3-min denaturation at 95°C, followed by 40 cycles at 95°C for 15 s, 60°C for 30 s, and 72°C for 30 s. After amplification, melting curves were analysed in each run to verify the amplification specificity of PCR products. An overview of the real-time qPCR program is presented in Table 7.

Table 7. The program of real-time qPCR

Program	Temperature	Duration	Number of cycles
Initial denaturation	95°C	3 min	1
Denaturation	95°C	15 s	40
Annealing	60°C	30 s	

Elongation	72°C	30 s	
A melt curve generated by heating from 60°C to 95°C with 0.2°C increments			

The relative mRNA expression level of each target gene was calculated using the comparative cycle threshold (CT) method ($2^{-\Delta\Delta CT}$), and the housekeeping gene glyceraldehyde 3-phosphate dehydrogenase (GAPDH) served as an internal reference for normalization. Specific primer sequences for PCR amplification in the current study are provided in Table 8 (Invitrogen, Darmstadt, Germany).

Table 8. List of the primers used in the study

Primer	Orientation	Sequence	Species
GAPDH	Forward	5'-TCAAGGCTGAGAACGGGAAG-3'	Human
GAPDH	Reverse	5'-TGGACTCCACGACGTACTCA-3'	Human
CaSR	Forward	5'-ATGCCAAGAAGGGAGAAAGACTCTT-3'	Human
CaSR	Reverse	5'-TCAGGACACTCCACACACTCAAAG-3'	Human
NFAT5	Forward	5'-GGGTCAAACGACGAGATTGTG-3'	Human
NFAT5	Reverse	5'-GTCCGTGGTAAGCTGAGAAAG-3'	Human
SGK1	Forward	5'-AGGAGGATGGGTCTGAACGA-3'	Human
SGK1	Reverse	5'-GGGCCAAGGTTGATTTGCTG-3'	Human
ORAI1	Forward	5'-CACCTGTTTGCGCTCATGAT-3'	Human
ORAI1	Reverse	5'-GGGACTCCTTGACCGAGTTG-3'	Human
ORAI2	Forward	5'-CAGCTCCGGGAAGGAACGTC-3'	Human
ORAI2	Reverse	5'-CTCCATCCCATCTCCTTGCG-3'	Human
ORAI3	Forward	5'-CTTCCAATCTCCCACGGTCC-3'	Human
ORAI3	Reverse	5'-GTTCCTGCTTGTAGCGGTCT-3'	Human
STIM1	Forward	5'-AAGAAGGCATTACTGGCGCT-3'	Human
STIM1	Reverse	5'-GATGGTGTGTCTGGGTCTGG-3'	Human
STIM2	Forward	5'-AGGGGATTCGCCTGTAACTG-3'	Human
STIM2	Reverse	5'-GGTTTACTGTCGTTGCCAGC-3'	Human

2.2.3 Immunoblotting

Conventional immunoblotting was performed to determine the protein abundance of ORAI1, STIM1 and GAPDH under various treatment conditions. For this purpose, proteins were extracted from cells, separated using gel electrophoresis, transferred onto PVDF membranes, incubated with specific antibodies and detected by ECL reagents. All of the steps are described in greater detail below.

2.2.3.1 Sample preparation

To prepare samples for electrophoresis, cells were lysed to release total proteins. Before protein extraction, RIPA lysis buffer (Cell Signalling Technology, Danvers, MA, USA) was supplemented with protease inhibitor cocktail (Thermo-Fisher Scientific, Waltham, MA, USA), which effectively inhibits serine-proteases, cysteine-proteases, aspartic acid-proteases and aminopeptidases to minimize proteolytic degradation during cell lysis and protein extraction. The composition of RIPA buffer is given in Table 9. Megakaryocytes were harvested and washed twice with ice-cold PBS. Then the pellet was suspended in 40 µL ice-cold RIPA buffer and incubated on ice for 30 min with gentle agitation every 5 min. After centrifugation for 20 min at 20,000 g and 4°C, the supernatant was collected for total protein concentration measurement using the Bradford assay (Bio-Rad Laboratories, Munich, Germany). The lysate was denatured by boiling at 100°C for 5 min following the addition of the loading buffer (Carl Roth, Karlsruhe, Germany).

Table 9. The composition of 1x RIPA buffer

Solution components	Concentration
Tris-HCl, pH 7.5	20 mM
NaCl	150 mM
Na_2EDTA	1 mM

EGTA	1 mM
NP-40	1%
Sodium deoxycholate	1%
Sodium pyrophosphate	2.5 mM
β-glycerophosphate	1 mM
Na_3VO_4	1 mM
Leupeptin	1 µg/ml

2.2.3.2 Gel electrophoresis

SDS–PAGE is a standard method for protein separation based on molecular weight. Polyacrylamide gels were composed of a lower 10% acrylamide resolving gel and an upper 5% acrylamide stacking gel, as detailed in Table 9. Equal amounts of protein samples (30 µg) were loaded into each gel lane and separated at a constant voltage of 80 V for 3 h until the dye front reached the bottom of the gel. A pre-stained protein ladder (Thermo-Fisher Scientific, Waltham, MA, USA) was run alongside the samples as a reference to estimate protein sizes.

Table 10. Solutions for preparing SDS-PAGE gels (sufficient for 2 gels)

Solution components	10% Resolving gels	5% Stacking gels
ddH_2O	5.9 mL	2.7 mL
30% Acrylamide/Bis-acrylamide	5.0 mL	670 µL
1.5 M Tris-HCl, pH 8.8	3.8 mL	-
1.0 M Tris-HCl, pH 6.8	-	500 µL
10% SDS	150 µL	40 µL
10% APS	150 µL	40 µL
TEMED	6 µL	4 µL
Total	15 mL	4 mL

2.2.3.3 Transfer of proteins and incubation

Size-separated proteins were immediately wet-transferred onto PVDF membranes (Bio-Rad Laboratories, Hercules, CA, USA) at a constant 100 V for

80 min. Following protein transfer, PVDF membranes were blocked with 5% non-fat milk (Carl Roth, Karlsruhe, Germany) in TBST for 1 h at room temperature and incubated overnight at 4°C with primary anti-ORAI1 antibody (1:1000, Proteintech, Chicago, IL, USA), anti-STIM1 antibody (Cell Signalling Technology, Danvers, MA, USA) and anti-GAPDH antibody (1:2000, Cell Signalling Technology, Danvers, MA, USA). After washing three times with TBST for 10 min each, the blots were incubated with HRP-conjugated anti-rabbit secondary antibody (1:2000, Cell Signalling Technology, Danvers, MA, USA) for 2 h at room temperature and washed again three times in TBST. Subsequently, protein bands were detected by ECL detection reagents (Thermo-Fisher Scientific, Waltham, MA, USA) and exposed to autoradiographic films (GE healthcare, Buckinghamshire, United Kingdom). For densitometry analysis, immunoblots were scanned, and band intensities were quantified using ImageJ software (Version 1.52, NIH, Bethesda, MD, USA). All of the results are presented as a ratio of target band intensity to GAPDH band intensity.

2.2.4 Intracellular Ca^{2+} imaging

2.2.4.1 Devices for intracellular Ca^{2+} imaging

The experimental setup for intracellular Ca^{2+} imaging is illustrated in figure 4.
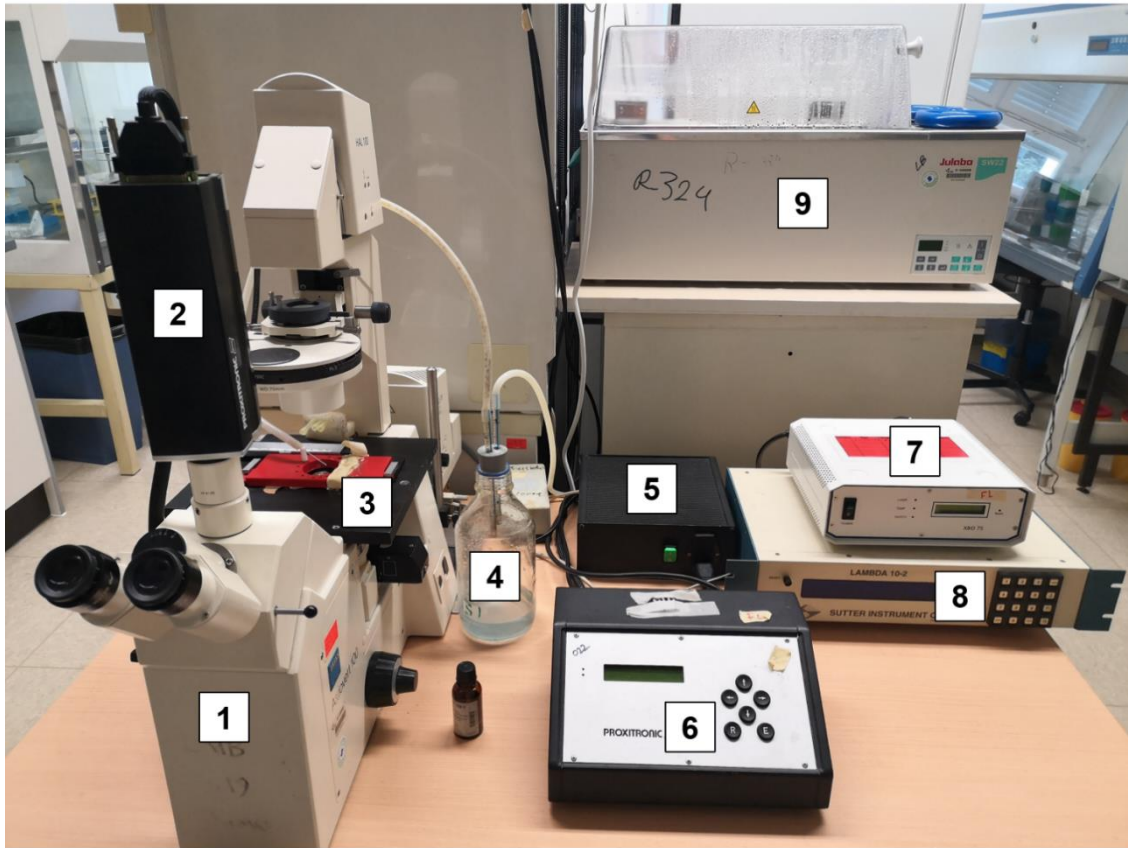
Figure 4. Intracellular Ca²⁺ imaging setup.
Divices are 1: inverted phase-contrast microscope; 2: camera; 3: perfusion chamber; 4: pump; 5: light source; 6: camera control panel; 7: lamp control panel; 8: filter wheel changer; 9: water bath.

2.2.4.2 Experimental procedure for intracellular Ca²⁺ imaging

Fluorescence imaging using Ca²⁺ indicator Fura-2/AM was employed to determine the intracellular Ca²⁺ concentration ($[Ca^{2+}]_i$). To this end, Meg-01 cells were plated on coverslips coated with poly-L-lysine (0.01%, Sigma-Aldrich, Steinheim, Germany). The cells were loaded with 2 µM Fura-2/AM (Invitrogen, Goettingen, Germany) in RPMI 1640 culture medium containing 10% FBS and 1% P/S for 30–45 min at 37°C. Once the incubation was accomplished, the coverslips were transferred to a perfusion chamber that was mounted on the stage of an inverted phase-contrast microscope (Axiovert 100, Zeiss, Oberkochen, Germany) equipped with a fluor 40×/1.30 oil immersion objective**.**

The emitted fluorescence intensity was detected at 505 nm every 10 s following dual excitation at 340 nm and 380 nm. Fluorescence images were acquired and quantified using the specialized software Metafluor (Version 7.5, Universal Imaging, Downingtown, PA, USA). To estimate cytosolic Ca^{2+} activity, changes in the 340/380 nm ratio were monitored at each time point after subtracting the background fluorescence. SOCE was determined upon intracellular Ca^{2+} store depletion by inhibiting sarco/endoplasmic reticulum Ca^{2+}-ATPase (SERCA) activity with 1 μM thapsigargin (Invitrogen, Goettingen, Germany) after extracellular Ca^{2+} removal, subsequently followed by Ca^{2+} re-addition in the constant presence of thapsigargin. The slopes (velocity, delta ratio/s) and peaks (magnitude, delta ratio) of the ratio increase were calculated for quantification of ER store depletion and Ca^{2+} entry, respectively. All measurements were performed at room temperature. In each experiment, fluorescent signals were obtained from 20–30 cells located in the field of view, and only those cells displaying distinct responses to thapsigargin and extracellular Ca^{2+} influx were included and then averaged for final data analyses. The standard HEPES solution and Ca^{2+}-free HEPES solution were prepared as described in Table 2.

2.3 Statistical analysis

All experimental data are presented as the means ± standard deviation (SD), and *n* values refer to the number of independent experiments (i.e., in experiments of intracellular Ca^{2+} imaging, the number of measured dishes). Data were analysed using SPSS software (Version 25.0, SPSS Inc., Chicago, IL, USA). The statistical significance was determined using two-tailed Student's *t* tests for comparisons between two groups. Ordinary one-way analysis of variance (ANOVA) was performed for multiple comparisons, followed by Tukey's post-hoc tests. A value of $p < 0.05$ was considered statistically significant.

3 Results

3.1 ORAI1 was the predominant ORAI isoform and STIM1 was the prevailing STIM isoform

Our qPCR analysis revealed that all three ORAI channel isoforms were detected in Meg-01 cells, in line with the results of previous reports (Pelzl et al., 2020). As shown in Figure 5A, *ORAI1* mRNA was the most abundant among the three isoforms. Both *ORAI2* and *ORAI3* were expressed at much lower levels, which suggests that ORAI1 is the predominant isoform present in Meg-01 cells. Likewise, *STIM1* and *STIM2* showed different expression levels. The *STIM1* mRNA was abundantly expressed in Meg-01 cells, whereas *STIM2* exhibited a lower mRNA expression (Figure 5B).
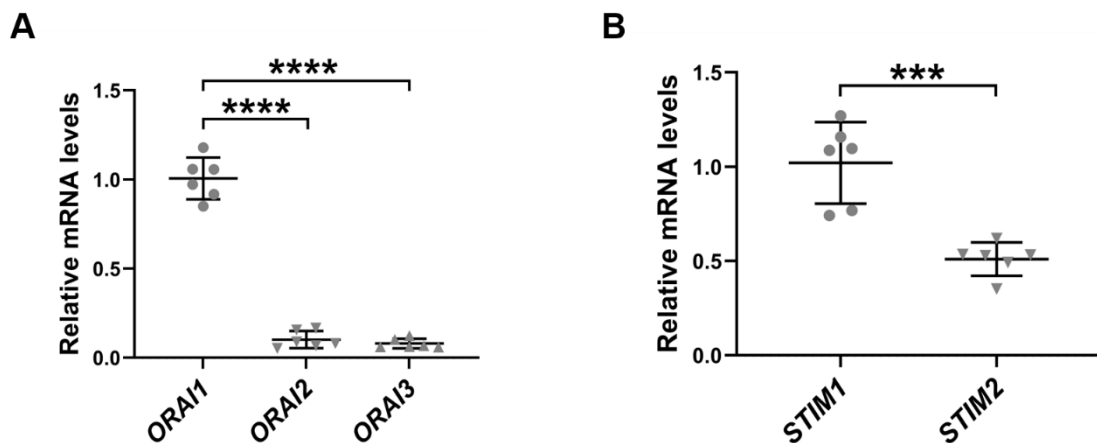

Figure 5. Relative transcript levels of *ORAI* and *STIM* isoforms in Meg-01 cells.
(A). Scatter plot showing the transcript levels of three *ORAI* isoforms in untreated megakaryocytes. The relative expression of *ORAI2* and *ORAI3* were normalized to *ORAI1*. **(B).** The mRNA expression of *STIM* isoforms under control conditions in megakaryocytes. The relative expression of *STIM2* was normalized to *STIM1*. Values refer to means ± SD. *n* = 6 per group. ***($p < 0.001$), ****($p < 0.0001$) indicate statistically significant differences from the group *ORAI1* or *STIM1* (ANOVA or Student's *t* test).

3.2 The appropriate concentration of MgCl$_2$ was 1.5 mM

In the first series of experiments, we examined the effects of MgCl$_2$ on

ORAI/STIM expression and SOCE activity in Meg-01 cells under high β-glycerophosphate conditions. To define the lowest concentration of $MgCl_2$ with effective suppression, Meg-01 cells were pre-incubated with increasing concentrations of $MgCl_2$ (0, 1.0, 1.5, and 2.0 mM) for 30 min, followed by 2 mM phosphate donor β-glycerophosphate stimulation for 24 h. Consistent with our earlier observations (Pelzl et al., 2020), *NFAT5*, *SGK1*, *ORAI1*, *ORAI2*, *ORAI3*, *STIM1* and *STIM2* levels were significantly enhanced at the transcript level in response to β-glycerophosphate treatment. Moreover, the mRNA levels of *NFAT5*, *SGK1*, *ORAI1*, *ORAI2*, *ORAI3*, *STIM1* and *STIM2* were diminished with increasing $MgCl_2$ concentrations. Figure 6 illustrates that all effects reached statistical significance at a concentration of 1.5 mM $MgCl_2$. As a result, 1.5 mM was selected as the optimal $MgCl_2$ concentration for the subsequent experiments.
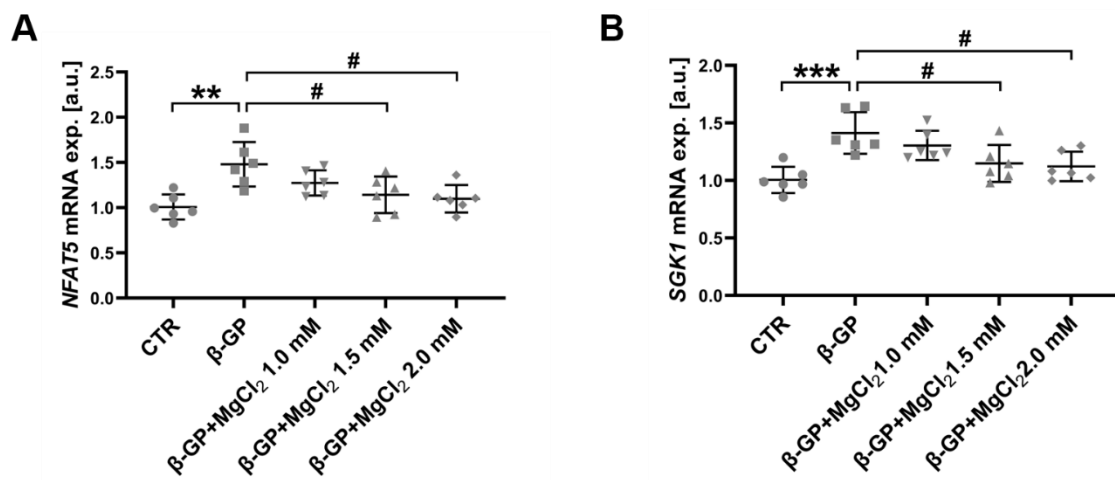
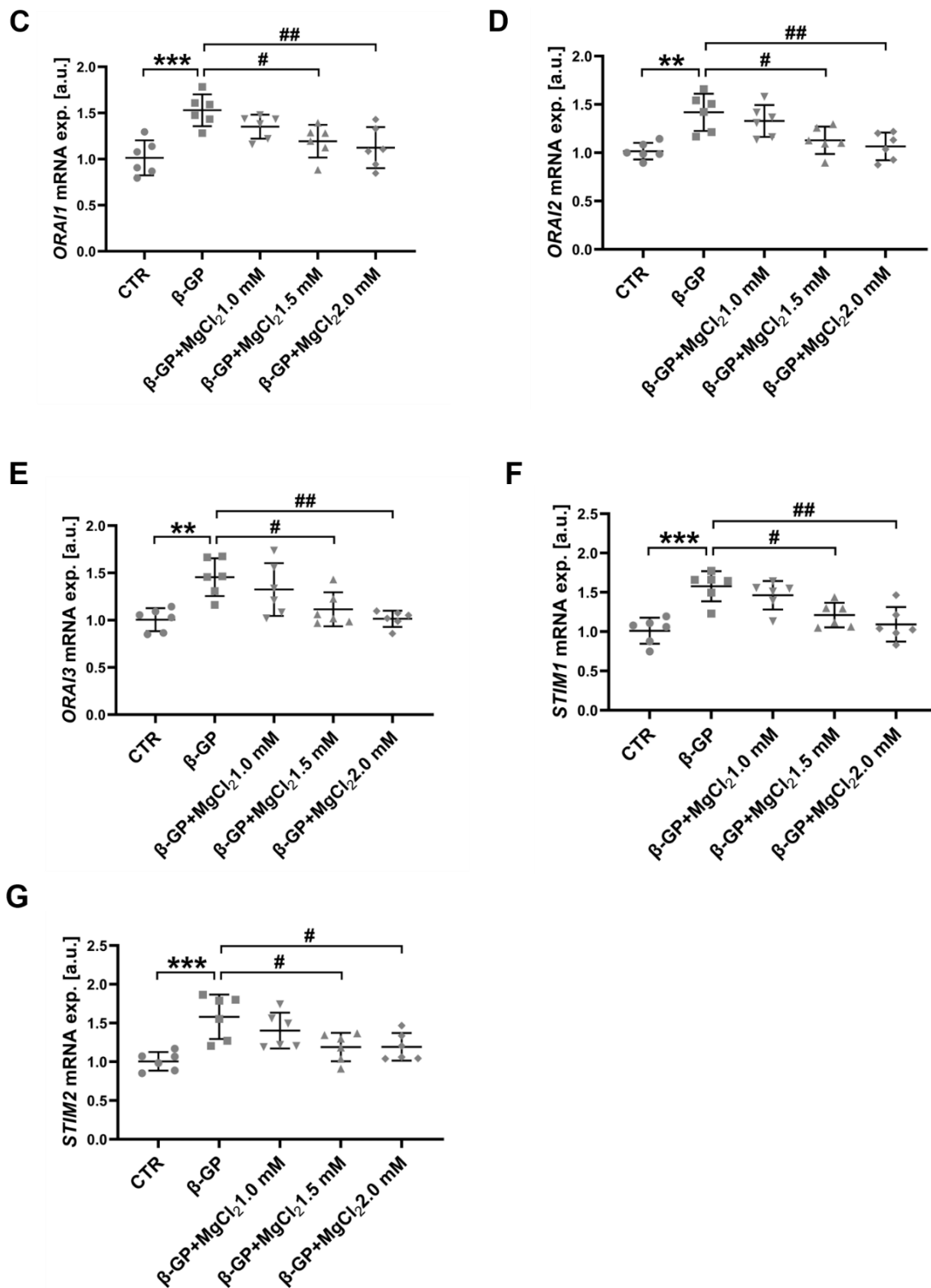**Figure 6. Effects of different concentrations of MgCl₂ on β-glycerophosphate-induced upregulation of *NFAT5, SGK1, ORAI1,2,3,* and *STIM1,2* transcription in megakaryocytes.**
(A-G). The mRNA expression of *NFAT5* **(A)**, *SGK1* **(B)**, *ORAI1* **(C)**, *ORAI2* **(D)**, *ORAI3* **(E)**, *STIM1* **(F)** and *STIM2* **(G)** in megakaryocytes exposed to various

concentrations of MgCl$_2$ (0, 1.0, 1.5, and 2.0 mM) for 30 min prior to a 24-h treatment with 2 mM β-glycerophosphate. Values refer to means ± SD. n = 6 per group. ** ($p < 0.01$), ***($p < 0.001$) indicate statistically significant differences from the CTR group; #($p < 0.05$), ##($p < 0.01$) indicate statistically significant differences from the β-GP group (ANOVA). CTR: control; NFAT5: nuclear factor of activated T cells 5; β-GP: β-glycerophosphate; SGK1: serum and glucocorticoid-inducible kinase 1; STIM1,2,3: stromal interaction molecule 1,2,3.

3.3 MgCl$_2$ counteracted β-glycerophosphate-triggered transcriptional elevation of *ORAI* and *STIM* isoform expression by activating CaSRs in Meg-01 cells

To testify whether CaSR activation is involved in regulating ORAI and STIM abundance, megakaryocytes were first exposed to MgCl$_2$ for 30 min and then incubated with β-glycerophosphate for 24 h. As indicated in Figure 7A, MgCl$_2$ treatment dramatically induced transcriptional upregulation of *CaSR* both in the absence and presence of β-glycerophosphate. We also assessed the inhibitory role of MgCl$_2$ in the signalling pathway stimulated by β-glycerophosphate. A 24 h pre-treatment of Meg-01 cells with 2 mM β-glycerophosphate apparently elevated the transcript levels of *NFAT5*, *SGK1*, *ORAI1*, *ORAI2*, *ORAI3*, as well as *STIM1* and *STIM2* (Figure 7B-H). Notably, all of these effects were remarkably attenuated upon the co-incubation of cells with 1.5 mM MgCl$_2$. In cells treated with MgCl$_2$ alone, the transcript levels of *NFAT5*, *SGK1*, *ORAI1*, *ORAI2*, *ORAI3*, *STIM1* and *STIM2* were not significantly modified.
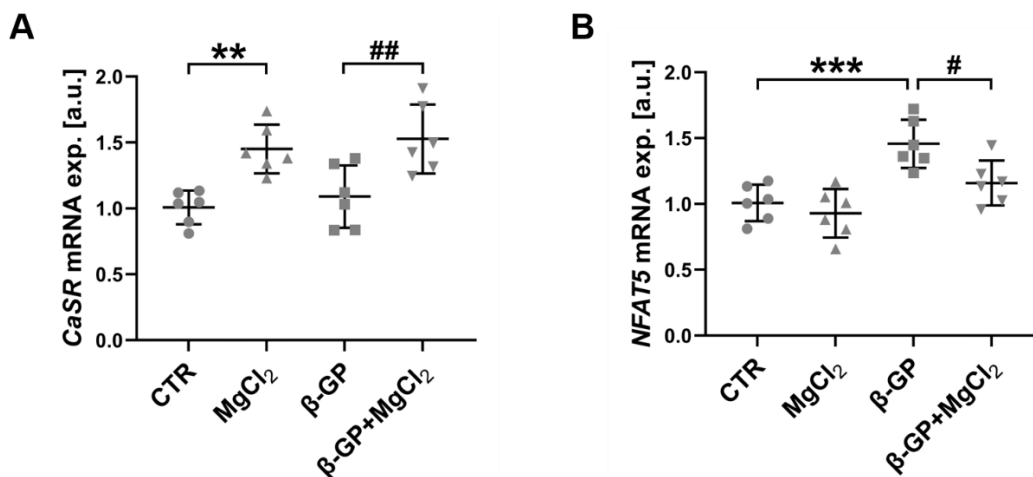
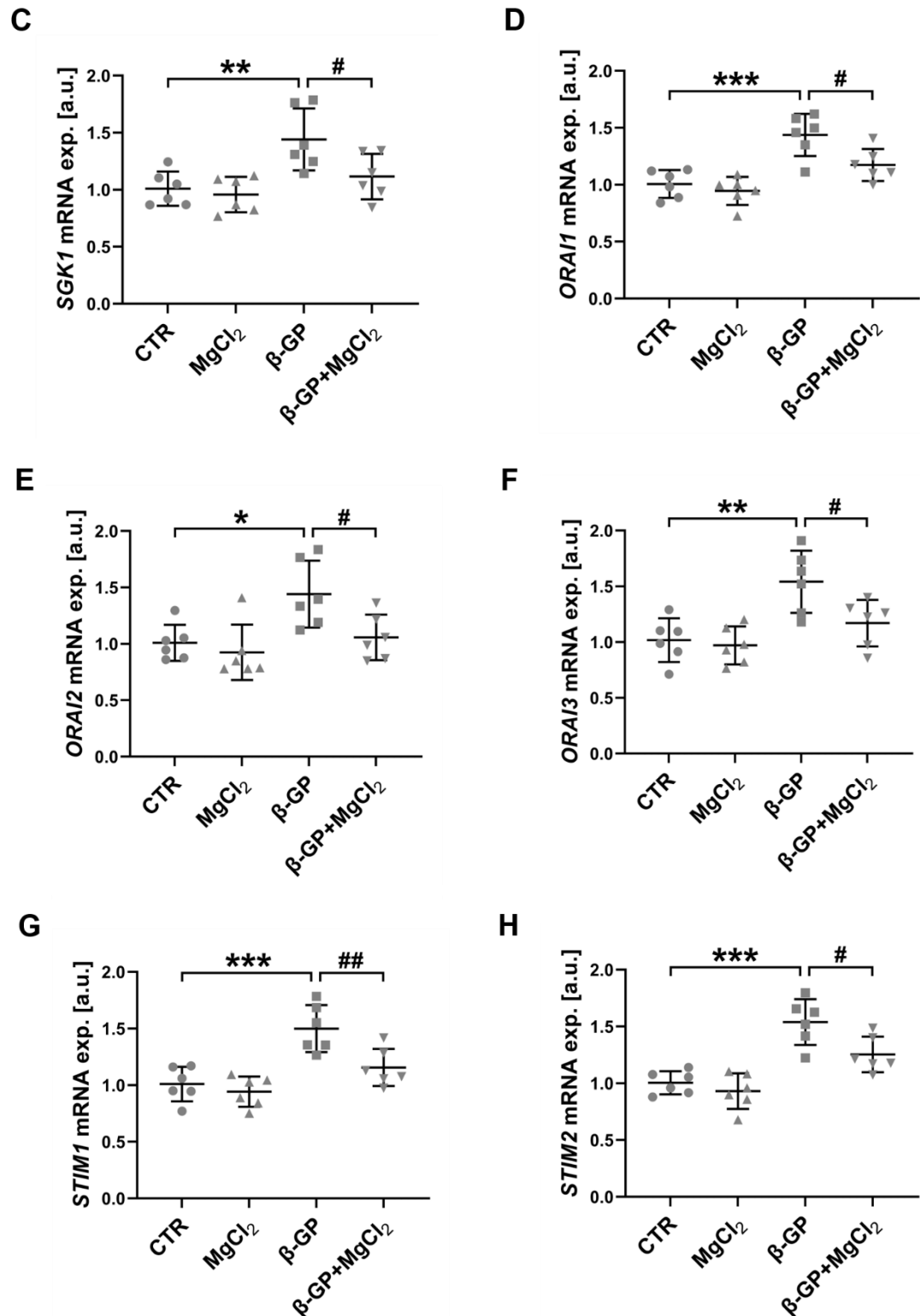**Figure 7. Upregulation of *CaSR* transcription by MgCl₂ and sensitivity of β-glycerophosphate-induced *NFAT5*, *SGK1*, *ORAI1,2,3*, and *STIM1,2* transcription to MgCl₂ in megakaryocytes.**

(A-H). The transcript levels of *CaSR* **(A)**, *NFAT5* **(B)**, *SGK1* **(C)**, *ORAI1* **(D)**, *ORAI2* **(E)**, *ORAI3* **(F)**, *STIM1* **(G)**, *STIM2* **(H)** in megakaryocytes following a 24-

h pre-treatment without (CTR) and with 2 mM β-glycerophosphate (β-GP) in the absence or presence of 1.5 mM $MgCl_2$. Values refer to means ± SD. $n = 6$ per group. *($p < 0.05$), ** ($p < 0.01$), ***($p < 0.001$) indicate statistically significant differences from the CTR group; [#]($p < 0.05$), [##]($p < 0.01$) indicate statistically significant differences from the β-GP group (ANOVA). CaSR: Ca^{2+}-sensing receptor; CTR: control; NFAT5: nuclear factor of activated T cells 5; β-GP: β-glycerophosphate; SGK1: serum and glucocorticoid-inducible kinase 1; STIM1,2,3: stromal interaction molecule 1,2,3.

3.4 Exposure to $MgCl_2$ reversed the upregulation of ORAI1 and STIM1 protein abundance by β-glycerophosphate in Meg-01 cells

Based on the fact that ORAI1 and STIM1 are the key molecular components of SOCE, we next investigated whether the alterations observed in *ORAI1* and *STIM1* transcript levels are accompanied by corresponding changes in the protein abundance. Immunoblot analysis implied that a 24-h β-glycerophosphate treatment was followed by an obvious increase in ORAI1 and STIM1 protein expression in Meg-01 cells, which was markedly blunted by additional treatment with 1.5 mM $MgCl_2$, as demonstrated in Figure 8. Moreover, $MgCl_2$ treatment did not significantly affect the ORAI1 and STIM1 protein levels in the absence of β-glycerophosphate.
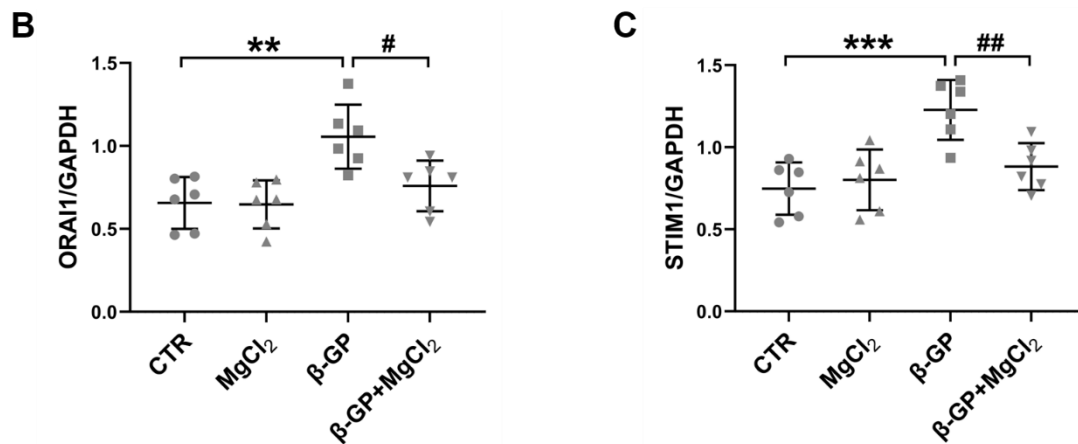
A

ORAI1		47
STIM1		89
GAPDH		37
	CTR MgCl₂ β-GP β-GP+ MgCl₂	(kDa)
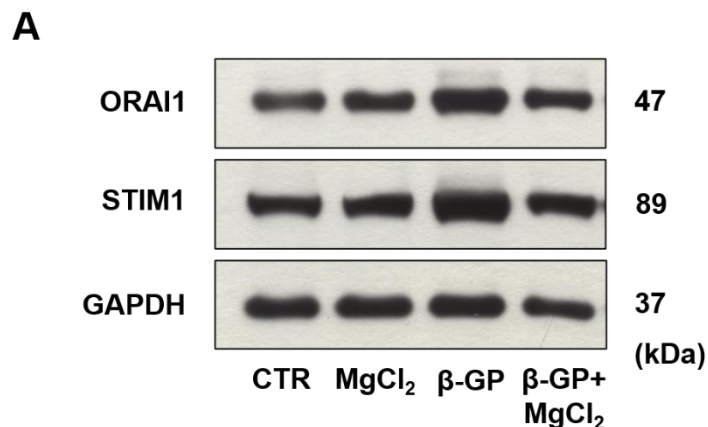
Figure 8. Sensitivity of β-glycerophosphate-induced ORAI1 and STIM1 protein expression to MgCl$_2$ in Meg-01 cells.
(A). Representative immunoblots showing protein abundance of ORAI1, STIM1 and GAPDH in megakaryocytes without (CTR) and with prior 24-h exposure to 2 mM β-glycerophosphate (β-GP) in the absence or presence of 1.5 mM MgCl$_2$. **(B,C).** Quantitative analyses of ORAI1 **(B)** and STIM1 **(C)** protein level following a 24-h incubation without (CTR) and with 2 mM β-glycerophosphate (β-GP) in the absence or presence of 1.5 mM MgCl$_2$ in megakaryocytes. Values refer to means ± SD. n = 6 per group. ** (p < 0.01), ***(p < 0.001) indicate statistically significant differences from the CTR group; [#](p < 0.05), [##](p < 0.01) indicate statistically significant differences from the β-GP group (ANOVA). CTR: control; GAPDH: glyceraldehyde 3-phosphate dehydrogenase; β-GP: β-glycerophosphate; STIM1: stromal interaction molecule 1.

3.5 MgCl$_2$ supplementation blunted the enhancement of SOCE by β-glycerophosphate in Meg-01 cells

To further explore whether the attenuation of the β-glycerophosphate-induced increase in ORAI1 and STIM1 abundance by MgCl$_2$ leads to SOCE suppression, Ca^{2+} imaging was conducted to monitor cytosolic Ca^{2+} activity ([Ca^{2+}]$_i$). Figure 9 displays that human megakaryocytes treated with 2 mM β-glycerophosphate (1.298 ± 0.086, n = 6) had slightly higher baseline levels than untreated cells (1.202 ± 0.094, n = 6) in a nominally Ca^{2+}-free solution, but the difference did not reach statistical significance. To empty intracellular Ca^{2+} stores, thapsigargin was applied to inhibit the SERCA pump and thereby generate a transient rise in the 340/380 mm ratio. Subsequently, the re-addition of extra Ca^{2+} elicited a sharp

increase, which was measured to characterize the thapsigargin-sensitive SOCE response. In the present study, pre-incubation with β-glycerophosphate caused a larger amplitude and shortened the time to reach the peak, and all effects were effectively suppressed by additional exposure to 1.5 mM $MgCl_2$ (Figure 9A,D,E). The peak value and the rate of ratio elevation following SOCE activation were not significantly modified by $MgCl_2$ treatment in the absence of β-glycerophosphate. Furthermore, neither β-glycerophosphate nor $MgCl_2$ significantly altered thapsigargin-evoked ER Ca^{2+} release (Figure 9A,B,C).
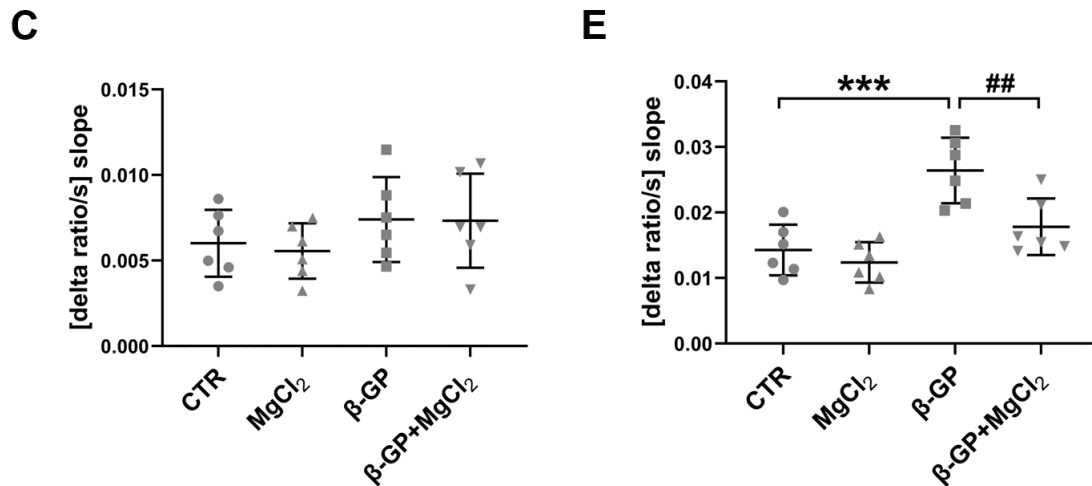
A

Calcium Release

SOCE

B

D
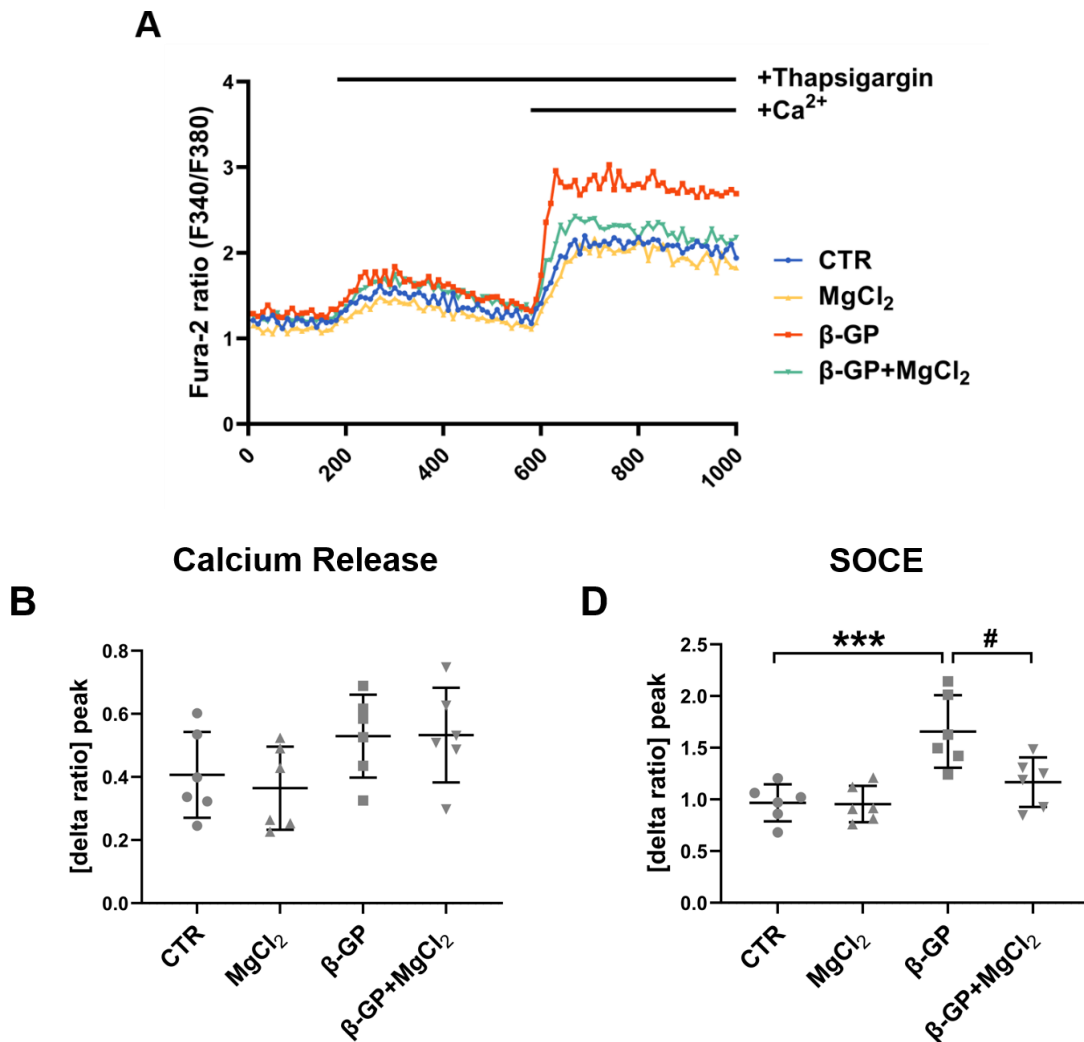
Figure 9. Sensitivity of β-glycerophosphate-induced SOCE to MgCl₂ in Meg-01 cells.

(A). Representative tracings of Fura-2/AM fluorescence-ratio reflecting cytosolic Ca^{2+} activity of Meg-01 cells before and following the exposure to SERCA pump inhibitor thapsigargin (1 μM) in the nominal absence of extracellular Ca^{2+} and subsequent extracellular Ca^{2+} addition (1 mM). Megakaryocytes were pre-treated without (CTR, blue) or with 1.5 mM MgCl₂ alone (MgCl₂, yellow), or 2 mM β-glycerophosphate alone (β-GP, red) or 2 mM β-glycerophosphate and 1.5 mM MgCl₂ (β-GP+MgCl₂, green) for 24 h. **(B,C).** The increase of Fura-2/AM fluorescence-ratio in the peak **(B)** and slope **(C)** after the addition of 1 μM thapsigargin into the Ca^{2+}-free HEPES solution in megakaryocytes without (CTR) and with 2 mM β-glycerophosphate treatment (β-GP) for 24 h in the absence or presence of 1.5 mM MgCl₂. **(D,E).** The increase of Fura-2/AM fluorescence-ratio in the peak **(D)** and slope **(E)** after the re-addition of 1 mM extracellular Ca^{2+} in megakaryocytes without (CTR) and with 2 mM β-glycerophosphate treatment (β-GP) for 24 h in the absence or presence of 1.5 mM MgCl₂. Values refer to means ± SD. *n* = 6 per group. ***($p < 0.001$) indicates a statistically significant difference from the CTR group; #($p < 0.05$), ##($p < 0.01$) indicate statistically significant differences from the Pi group (ANOVA). CTR: control; β-GP: β-glycerophosphate; SOCE: store-operated Ca^{2+} entry.

3.6 The optimal concentration of GdCl₃ was 50 μM

Our next series of experiments tested whether the inhibitory effects of MgCl₂ are mimicked by treatment with another Ca^{2+}-sensing receptor agonist, GdCl₃. To identify the lowest effective concentration of GdCl₃, Meg-01 cells were exposed to 2 mM β-glycerophosphate for 24 h in the absence or presence of GdCl₃ at various concentrations (10, 20, 50, and 100 μM). The results from qPCR analysis

presented that β-glycerophosphate-triggered transcriptional upregulation of *NFAT5*, *SGK1*, *ORAI1*, *ORAI2*, *ORAI3*, *STIM1* and *STIM2* levels was appreciably alleviated by GdCl₃ in a dose-dependent manner. At 20 µM, the upregulation of STIM1 levels induced by β-glycerophosphate was strongly reduced (Figure 10F), while the minimum inhibitory concentration in the genes *NFAT5*, *SGK1*, *ORAI1*, *ORAI2*, *ORAI3* and *STIM2* was 50 µM (Figure 10A-E,G). Taken together, these data suggested that a concentration of 50 µM was the most appropriate GdCl₃ concentration in the following experiments.
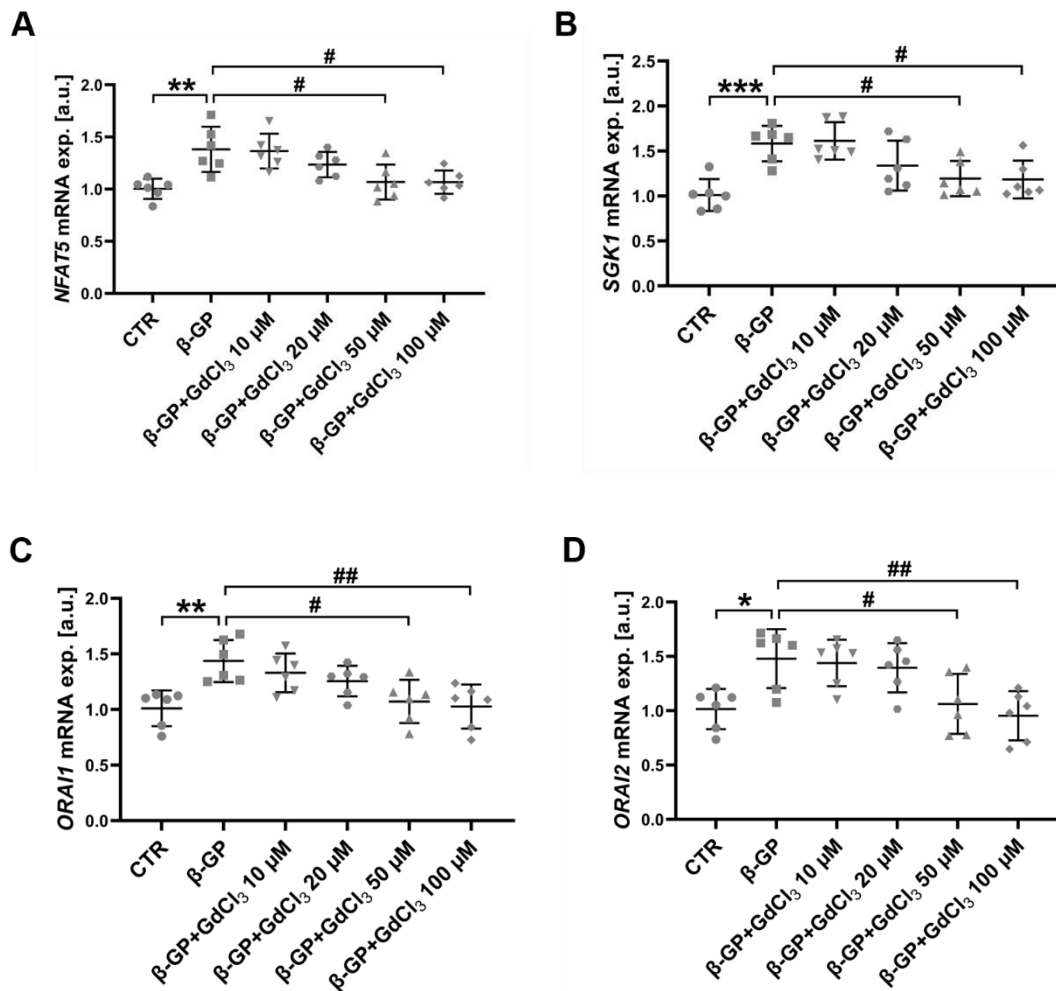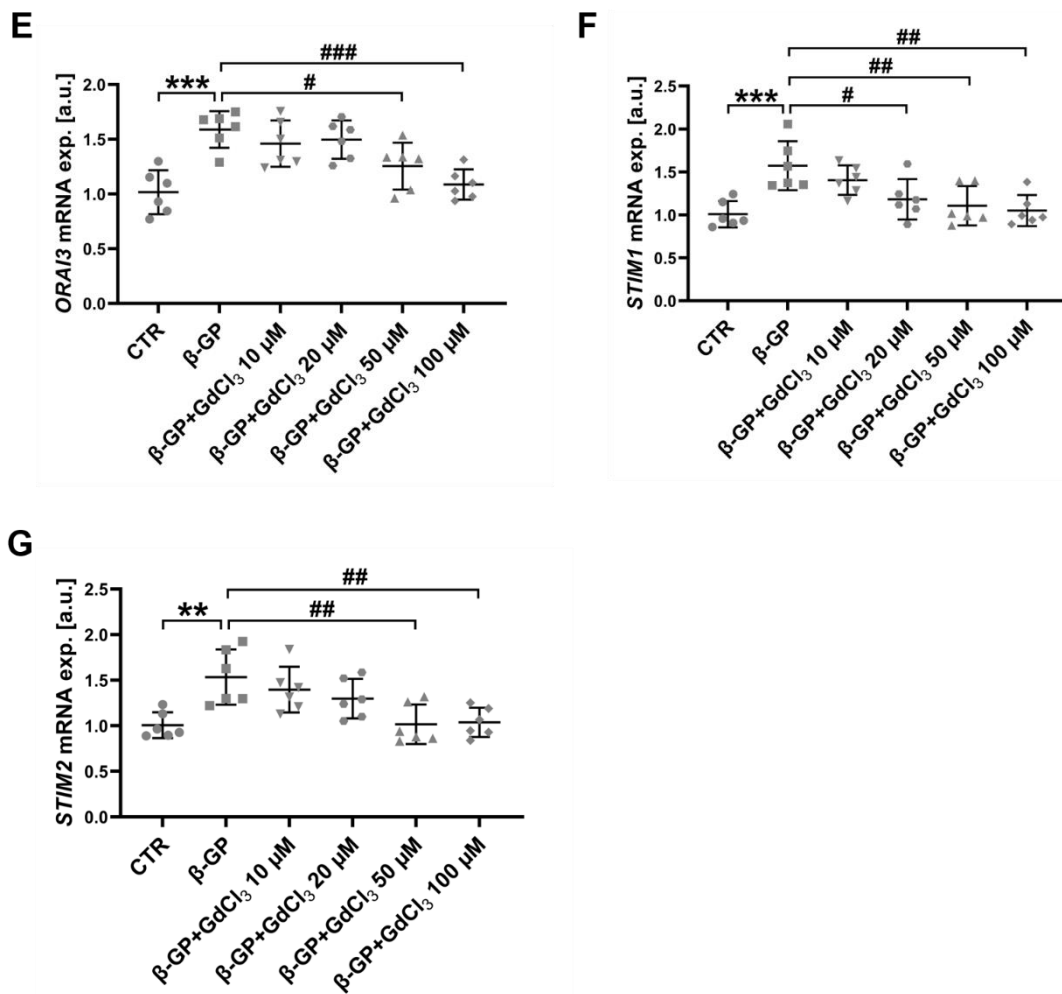
Figure 10. Effects of different concentrations of GdCl₃ on β-glycerophosphate-induced upregulation of *NFAT5, SGK1, ORAI1,2,3*, and *STIM1,2* transcription in megakaryocytes.
(A-G). The mRNA expression of *NFAT5* **(A)**, *SGK1* **(B)**, *ORAI1* **(C)**, *ORAI2* **(D)**, *ORAI3* **(E)**, *STIM1* **(F)** and *STIM2* **(G)** in megakaryocytes exposed to various concentrations of GdCl₃ (10, 20, 50, and 100 µM) for 30 min prior to a 24-h treatment with 2 mM β-glycerophosphate. Values refer to means ± SD. *n* = 6 per group. *($p < 0.05$), **($p < 0.01$), ***($p < 0.001$) indicate statistically significant differences from the CTR group; #($p < 0.05$), ##($p < 0.01$), ###($p < 0.001$) indicate statistically significant differences from the β-GP group (ANOVA). CTR: control; NFAT5: nuclear factor of activated T cells 5; β-GP: β-glycerophosphate; SGK1: serum and glucocorticoid-inducible kinase 1; STIM1,2,3: stromal interaction molecule 1,2,3.

3.7 The stimulatory effects of β-glycerophosphate on *ORAI* and *STIM* transcription were attenuated by GdCl₃ via activation of CaSRs in Meg-01 cells

We analysed multiple genes involved in the β-glycerophosphate-stimulated Ca^{2+} signalling pathway by utilizing qPCR. Pre-treatment with $GdCl_3$ enhanced CaSR mRNA expression in Meg-01 cells with or without β-glycerophosphate (Figure 11A). In addition, the transcriptional upregulation of *NFAT5*, *SGK1*, *ORAI1*, *ORAI2*, *ORAI3*, *STIM1* and *STIM2* expression induced by β-glycerophosphate was effectively prevented upon co-incubation with 50 µM $GdCl_3$ (Figure 11B-H). In the absence of β-glycerophosphate, treatment with $GdCl_3$ did not affect the transcript levels of *NFAT5*, *SGK1*, *ORAI1*, *ORAI2*, *ORAI3*, *STIM1* or *STIM2*.
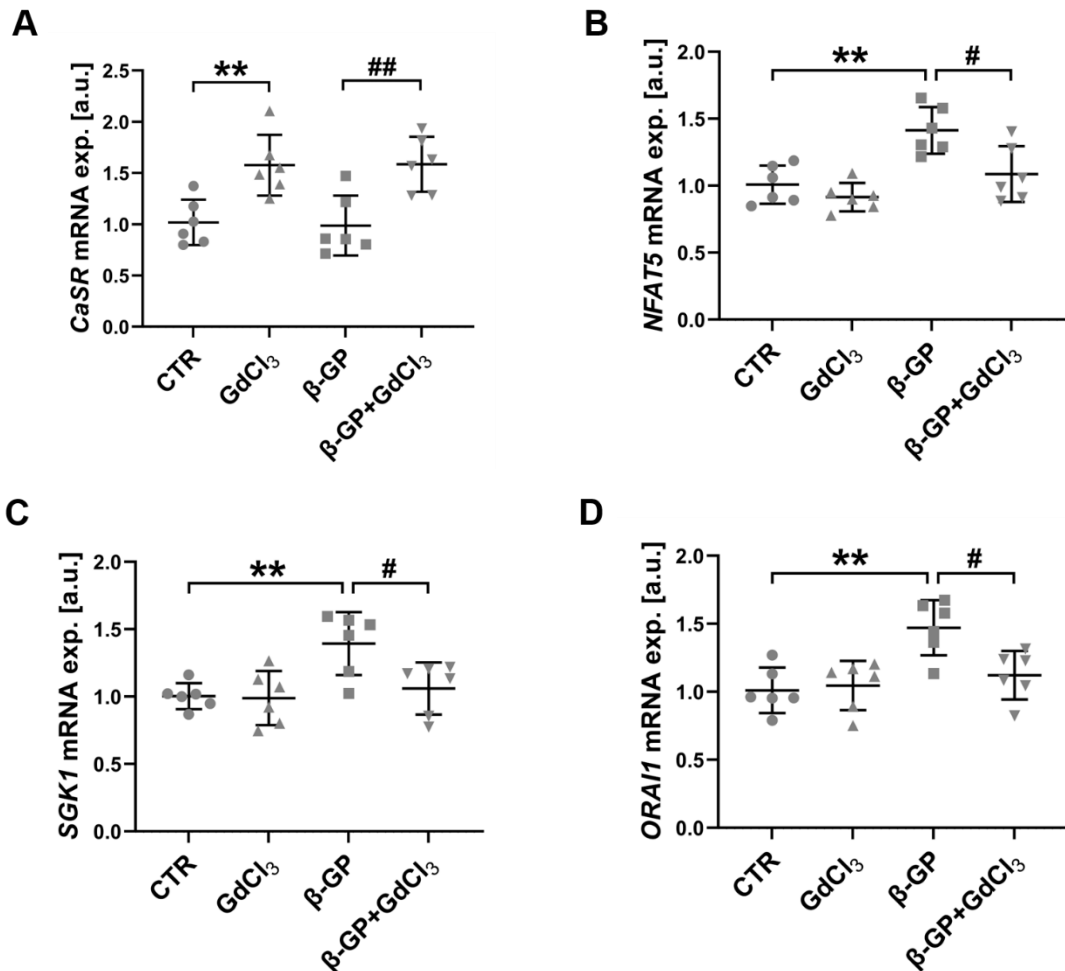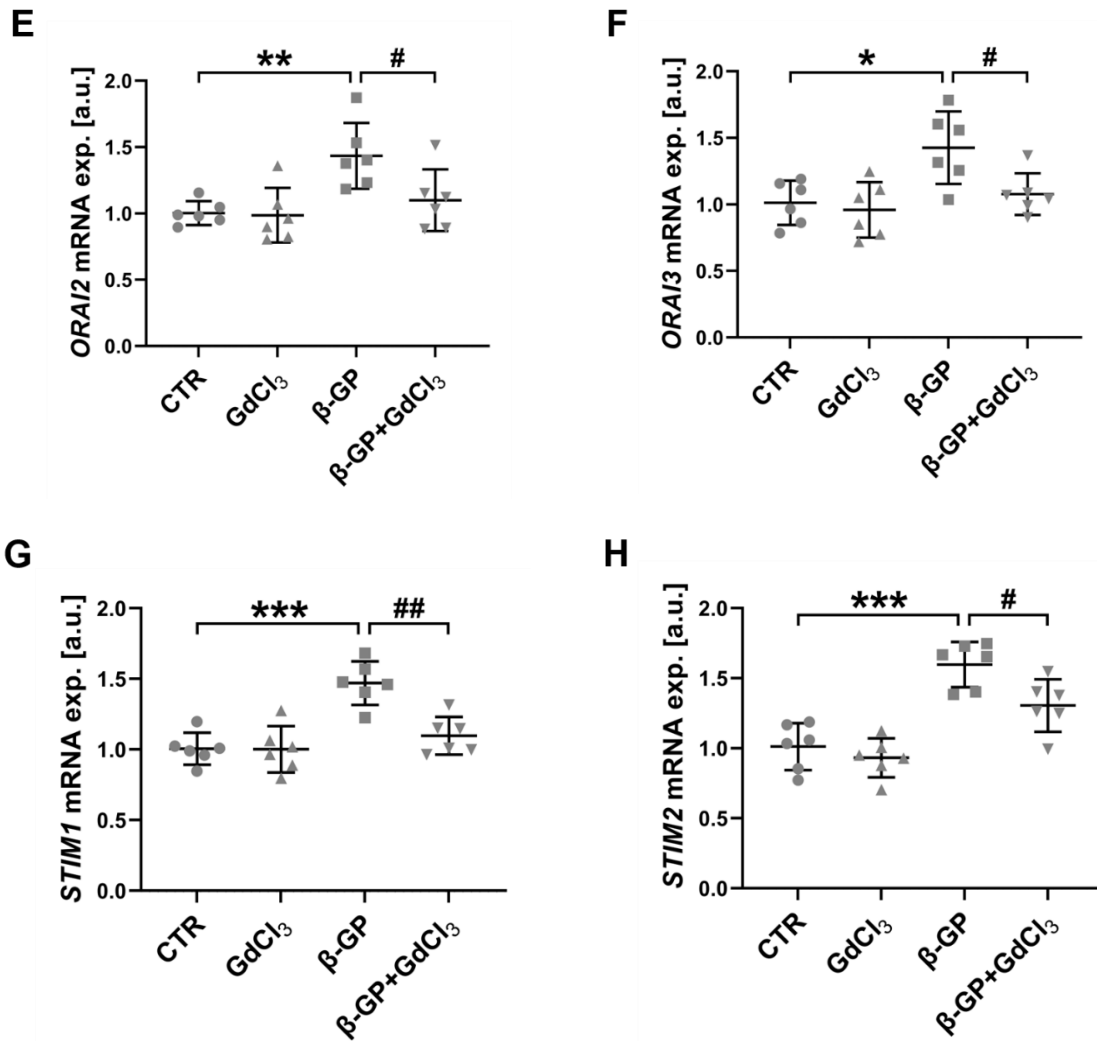
Figure 11. Upregulation of *CaSR* transcription by GdCl$_3$ and sensitivity of β-glycerophosphate-induced *NFAT5*, *SGK1*, *ORAI1,2,3*, and *STIM1,2* transcription to GdCl$_3$ in megakaryocytes.

(A-H). The transcript levels of *CaSR* **(A)**, *NFAT5* **(B)**, *SGK1* **(C)**, *ORAI1* **(D)**, *ORAI2* **(E)**, *ORAI3* **(F)**, *STIM1* **(G)**, *STIM2* **(H)** in megakaryocytes following a 24-h pre-treatment without (CTR) and with 2 mM β-glycerophosphate (β-GP) in the absence or presence of 50 µM GdCl$_3$. Values refer to means ± SD. *n* = 6 per group. *($p < 0.05$), ** ($p < 0.01$), ***($p < 0.001$) indicate statistically significant differences from the CTR group; #($p < 0.05$), ##($p < 0.01$) indicate statistically significant differences from the β-GP group (ANOVA). CaSR: Ca^{2+}-sensing receptor; CTR: control; NFAT5: nuclear factor of activated T cells 5; β-GP: β-glycerophosphate; SGK1: serum and glucocorticoid-inducible kinase 1; STIM1,2,3: stromal interaction molecule 1,2,3.

3.8 GdCl$_3$ modified the elevation of ORAI1 and STIM1 protein abundance by β-glycerophosphate in Meg-01 cells

Immunoblotting was performed to check whether the altered transcript abundance of *ORAI1* and *STIM1* is paralleled by respective changes in protein content. In Meg-01 cells pre-treated with β-glycerophosphate, there were markedly higher ORAI1 and STIM1 protein expression levels than those in the control-cultured cells, which was significantly counteracted by additional exposure to 50 µM GdCl$_3$ (Figure 12). In addition, ORAI1 and STIM1 protein abundance remained unaffected when cells were treated with GdCl$_3$ alone.
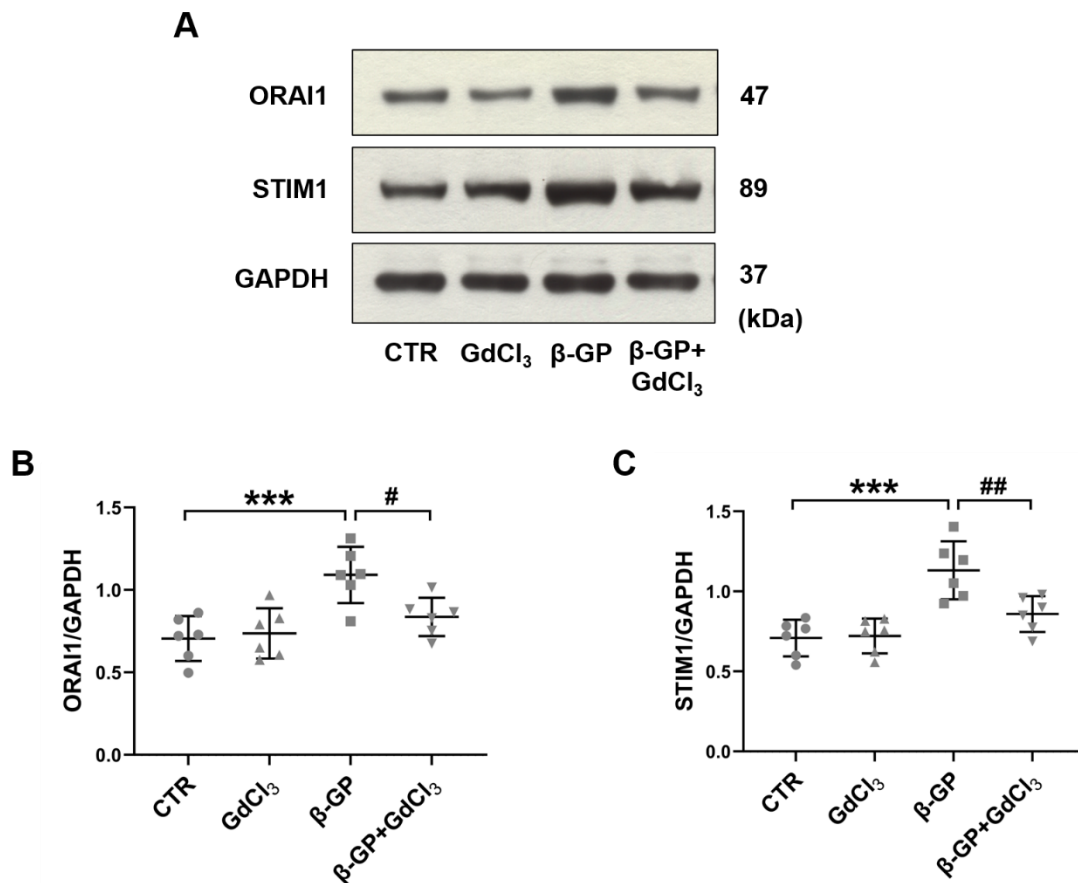
Figure 12. Sensitivity of β-glycerophosphate-induced ORAI1 and STIM1 protein expression to GdCl$_3$ in Meg-01 cells.
(A). Representative immunoblots showing protein abundance of ORAI1, STIM1 and GAPDH in megakaryocytes without (CTR) and with prior 24-h exposure to 2 mM β-glycerophosphate (β-GP) in the absence or presence of 50 µM GdCl$_3$. **(B,C).** Quantitative analyses of ORAI1 **(B)** and STIM1 **(C)** protein level following

a 24-h incubation without (CTR) and with 2 mM β-glycerophosphate (β-GP) in the absence or presence of 50 µM GdCl$_3$ in megakaryocytes. Values refer to means ± SD. n = 6 per group. ***($p < 0.001$) indicates a statistically significant difference from the CTR group; #($p < 0.05$), ##($p < 0.01$) indicate statistically significant differences from the β-GP group (ANOVA). CTR: control; GAPDH: glyceraldehyde 3-phosphate dehydrogenase; β-GP: β-glycerophosphate; STIM1: stromal interaction molecule 1.

3.9 GdCl$_3$ treatment suppressed the enhancement in SOCE activity by β-glycerophosphate in Meg-01 cells

At last, we sought to determine the influence of GdCl$_3$ in inhibiting β-glycerophosphate-induced SOCE enhancement through intracellular Ca^{2+} imaging. Our results exhibit that 50 µM GdCl$_3$ remarkably reversed the elevation of SOCE under high β-glycerophosphate conditions, both in slope and peak (Figure 13A,D,E). There were no notable changes observed in SOCE activity without additional exposure to β-glycerophosphate. Again, neither β-glycerophosphate nor GdCl$_3$ significantly modified thapsigargin-mediated internal Ca^{2+} store release (Figure 13A,B,C).
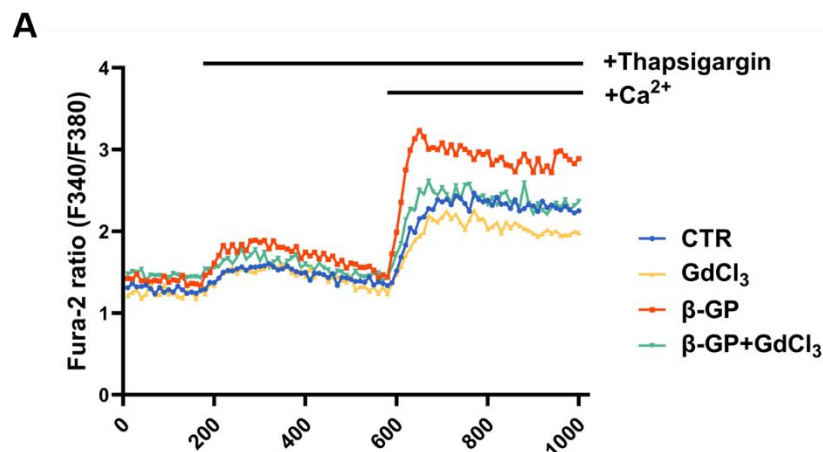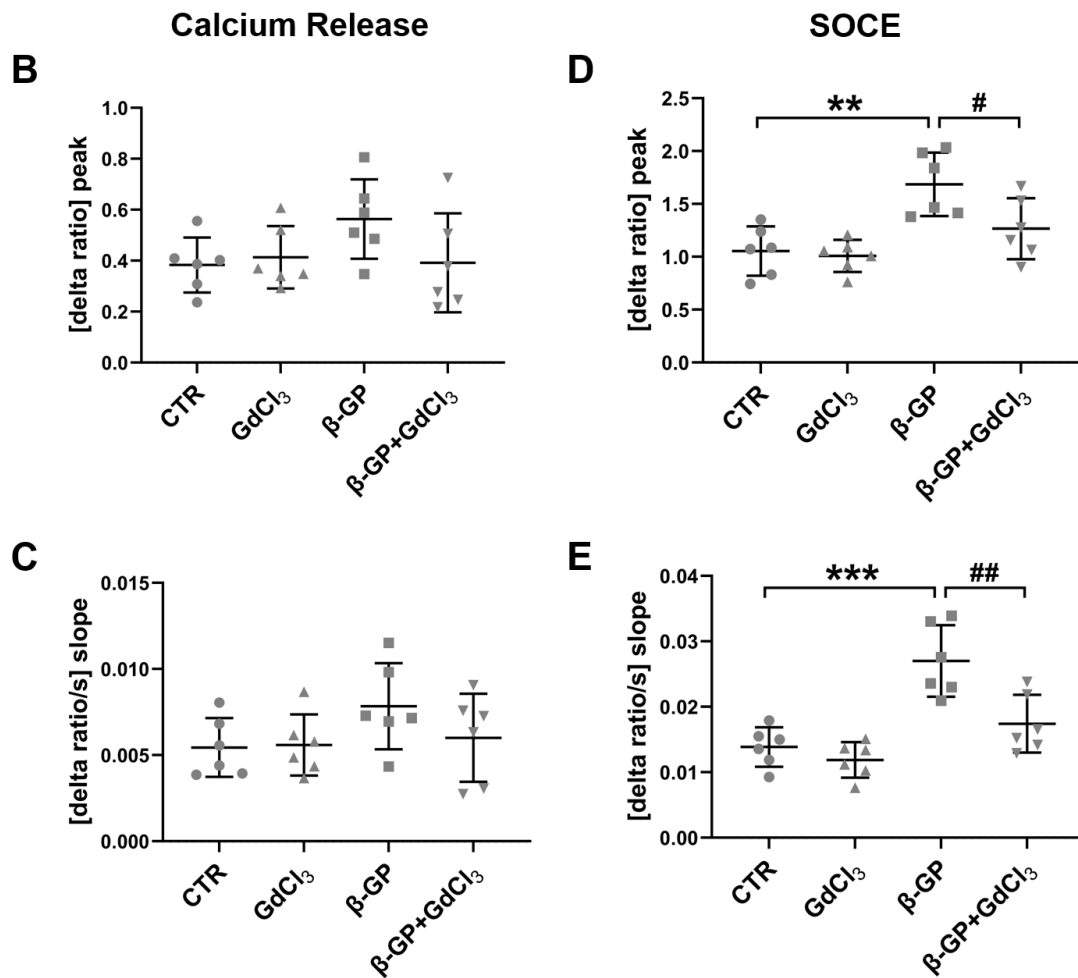
Figure 13. Sensitivity of β-glycerophosphate-induced SOCE to GdCl₃ in Meg-01 cells.

(A). Representative tracings of Fura-2/AM fluorescence-ratio reflecting cytosolic Ca^{2+} activity of Meg-01 cells before and following the exposure to SERCA pump inhibitor thapsigargin (1 µM) in the nominal absence of extracellular Ca^{2+} and subsequent extracellular Ca^{2+} addition (1 mM). Megakaryocytes were pre-treated without (CTR, blue) or with 50 µM GdCl₃ alone (GdCl₃, yellow), or 2 mM β-glycerophosphate alone (β-GP, red) or 2 mM β-glycerophosphate and 50 µM GdCl₃ (β-GP+GdCl₃, green) for 24 h. **(B,C).** The increase of Fura-2/AM fluorescence-ratio in the peak **(B)** and slope **(C)** after the addition of 1 µM thapsigargin into the Ca^{2+}-free HEPES solution in megakaryocytes without (CTR) and with 2 mM β-glycerophosphate treatment (β-GP) for 24 h in the absence or presence of 50 µM GdCl₃. **(D,E).** The increase of Fura-2/AM fluorescence-ratio in the peak **(D)** and slope **(E)** after the re-addition of 1 mM extracellular Ca^{2+} in megakaryocytes without (CTR) and with 2 mM β-glycerophosphate treatment (β-GP) for 24 h in the absence or presence of 50 µM GdCl₃. Values refer to means ± SD. n = 6 per group. **($p < 0.01$), ***($p < 0.001$) indicate statistically significant

differences from the CTR group; [#]($p < 0.05$), [##]($p < 0.01$) indicate statistically significant differences from the β-GP group (ANOVA). CTR: control; β-GP: β-glycerophosphate; SOCE: store-operated Ca^{2+} entry.

4 Discussion

NFAT5, SGK1, ORAI and STIM isoforms similarly participate in the activation of circulating platelets (Lang et al., 2013, Borst et al., 2012, Zhou et al., 2021, Pelzl et al., 2020), which contributes to the increased risk of developing thrombosis and subsequent thrombo-occlusive events. As described before, megakaryocytes undergo a complex differentiation process and convert their cytoplasm into long branched pro-platelets that yield individual platelets into the bloodstream (Patel et al., 2005, Italiano et al., 1999). Considering that the abundance of respective proteins in platelets depends on megakaryocytic transcript and protein synthesis, we give special attention to the molecular regulation in megakaryocytes.
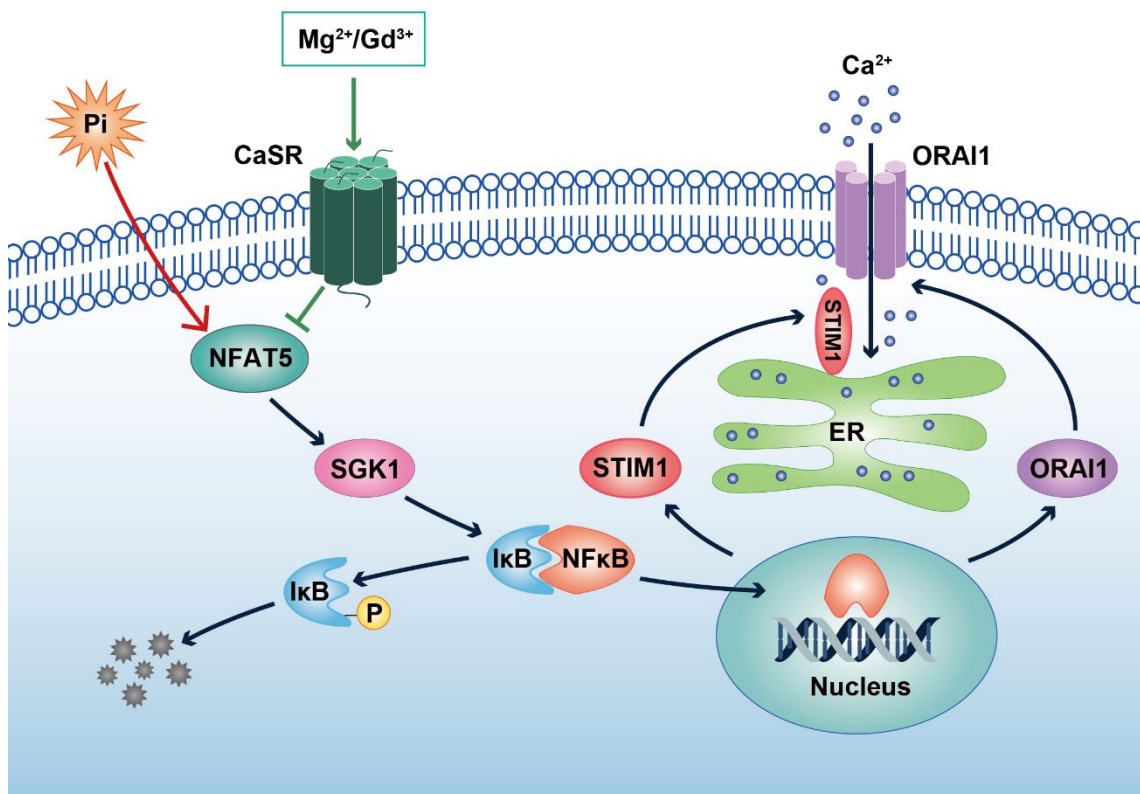

Figure 14. Mg^{2+} and Gd^{3+} suppress phosphate-stimulated ORAI1/STIM1 upregulation and SOCE enhancement via the activation of CaSRs in megakaryocytes–a schematic representation (from Zhou et al., 2021).
In megakaryocytes, the phosphate donor β-glycerophosphate upregulates the

expression of NFAT5 and SGK1, which results in the degradation of the NF-κB inhibitory protein IκB, the nuclear translocation of NFκB and NFκB-dependent transcription of *ORAI1* and *STIM1*. Mg^{2+} and Gd^{3+} attenuate the enhancement of SOCE mediated by phosphate, at least partially via CaSR activation and subsequent downregulation of this signalling cascade. CaSR: Ca^{2+}-sensing receptor; ER: endoplasmic reticulum; NFAT5: nuclear factor of activated T cells 5; NF-κB: nuclear factor-κB; Pi: inorganic phosphate; SGK1: serum and glucocorticoid-inducible kinase 1; STIM1: stromal interaction molecule1.

The present study supports earlier observations that the exposure of human megakaryocytes to the phosphate donor β-glycerophosphate stimulates transcript upregulation of *NFAT5*, *SGK1*, *ORAI1*, *ORAI2*, *ORAI3*, *STIM1* and *STIM2* expression as well as SOCE (Pelzl et al., 2020). Notably, the present study further testifies that all of these effects were strongly attenuated or abolished by 1.5 mM $MgCl_2$ and the 50 μM CaSR agonist $GdCl_3$. A schematic diagram summarizing our findings is provided in Figure 14.

4.1 Store-operated Ca^{2+} entry

The rise in cytosolic Ca^{2+} concentration is recognized as a central event in mediating platelet functions during the process of thrombus formation and haemostasis (Davies et al., 1989). A continuously growing body of evidence suggests that the main pathway of Ca^{2+} entry into platelets is SOCE, where the Ca^{2+} sensor STIMs and CRAC channel pore-forming subunit ORAIs are the primary elements participating in Ca^{2+} signalling in platelet activation (Harper and Poole, 2011, Berna-Erro et al., 2016). All three ORAI homologues function similarly in coupling to STIM isoforms following ER Ca^{2+} store depletion, causing an increase in inwardly rectifying Ca^{2+} currents (Wang et al., 2017a, Prakriya, 2013). The differences between these isoforms need to be clarified.

To date, ORAI1 is the best-known isoform highly expressed in a variety of immune cells, such as macrophages, T cells and B cells, as well as non-immune cells, such as platelets, endothelial cells and hepatocytes (Prakriya and Lewis,

2015, Nguyen et al., 2018). Mercer JC et al. demonstrated that the magnitude of ORAI2-dependent currents was smaller than that obtained in ORAI1 when co-expressed with STIM1, while ORAI3 was able to rescue Ca^{2+} entry after siRNA knockdown of *ORAI1* (Mercer et al., 2006). These ORAI proteins are capable of constituting or augmenting SOCE in a rank order of efficacy of ORAI1 > ORAI2 > ORAI3.

STIM1 and STIM2 are highly homologous in amino acid sequences and domain architecture (Williams et al., 2001), but they harbour some differences that may be responsible for their distinct physiological functions. Recent studies have provided compelling evidence establishing STIM1 as the main Ca^{2+} sensor that communicates between the filling state of internal stores and Ca^{2+} channels in the PM. However, it should be noted that STIM1 merely responds to the pronounced degree of store depletion, although it gets activated rapidly and triggers considerably large Ca^{2+} influx (Grabmayr et al., 2020). The STIM2 EF-hand displays a lower binding affinity for Ca^{2+} than that of STIM1, which makes it more sensitive to minor fluctuations in ER luminal Ca^{2+} levels (Nguyen et al., 2018). Therefore, it is not surprising that, upon a small reduction in ER Ca^{2+} content, STIM2 triggers slow but sustained SOCE as a compensation for the slight store depletion (Zhou et al., 2009, Grabmayr et al., 2020), which indicates that STIM2 functions as a regulator in the feedback system stabilizing basal cytoplasmic and ER Ca^{2+} concentrations (Brandman et al., 2007).

The present study found that both the CRAC ion channels ORAI1, ORAI2, ORAI3 and the ER-localized Ca^{2+} sensor isoforms STIM1, STIM2 were expressed in human megakaryocytes. According to qPCR results, ORAI1 was the prevailing ORAI isoform and STIM1 was the predominant STIM isoform involved in activating SOCE function. A previous study demonstrated that platelets from *Orai1*^{-/-} mice were characterized by severely defective SOCE,

impaired agonist-induced increase in Ca^{2+} and reduced thrombus formation under flow *in vitro*. (Braun et al., 2009). Additionally, STIM1-deficient platelets showed abrogated SOCE as a consequence of defective glycoprotein VI collagen receptor (GPVI)-mediated Ca^{2+} signalling. These platelets also displayed diminished collagen-induced PS exposure and GPVI-stimulated procoagulant activity, presumably due to their impaired agonist responses (Gilio et al., 2010, Ahmad et al., 2011, Varga-Szabo et al., 2008). The similar results observed in *Orai1*^{-/-} or *Stim1*^{-/-} platelets indicated that these two molecules work jointly in the same Ca^{2+} signalling pathway and revealed the prominent role of SOCE in thrombus generation and stabilization. Nevertheless, additional efforts are needed to clarify the contribution of ORAI2, ORAI3 and STIM2 to SOCE function and the activation of blood platelets.

4.2 Signalling cascade of NFAT5/SGK1/ORAIs/STIMs

NFAT5, originally cloned as a tonicity-regulated transcription factor enhanced by hyperosmotic cell shrinkage (Cheung and Ko, 2013), is upregulated in hyperphosphatemic CKD patients, which in turn induces the expression of SGK1 (Chen et al., 2009). SGK1 acts as a powerful stimulator of the Ca^{2+} channel ORAI1/STIM1 and thus enhances the sensitivity of platelets to agonists of Ca^{2+} entry, resulting in the degranulation, aggregation and thrombus formation of circulating platelets (Lang et al., 2017). SGK1-sensitive ORAI1/STIM1 expression is partially mediated via NF-κB activity. By phosphorylating NF-κB inhibitory protein IκB kinase (IKKα/β), SGK1 facilitates the phosphorylation of IκB with the subsequent degradation of IκB, the nuclear translocation of NF-κB subunits and NF-κB-dependent transcription of both *ORAI1* and *STIM1* (Borst et al., 2012, Lang et al., 2013). SGK1 is further effective by disrupting the action of Nedd4–2, a ubiquitin ligase driving the ubiquitination and proteasomal degradation of several channel proteins including ORAI1 (Lang and Shumilina, 2013). The

expression of SGK1 and SGK1-sensitive upregulation of ORAI1 is stimulated by diverse triggers, involving ischaemia, oxidative stress, excessive glucose concentration, radiation, DNA damage, and a variety of factors, including glucocorticoids, mineralocorticoids, fibroblast growth factor, transforming growth factor beta (TGF-β), thrombin, advanced glycation end products (AGEs), as well as platelet-derived growth factor (PDGF) (Lang et al., 2006, Lang and Voelkl, 2013, Lang et al., 2018). Through megakaryocytic NF-κB induction and ORAI1/STIM1 upregulation, SGK1 stimulation leads to enhanced SOCE, which predisposes CKD patients to thrombosis and stroke.

In agreement with prior observations, our results demonstrated that the transcript levels of *NFAT5*, *SGK1*, *ORAI1*, *ORAI2*, *ORAI3*, *STIM1* and *STIM2* were significantly upregulated by 2 mM phosphate-donor β-glycerophosphate in human megakaryocytes (Pelzl et al., 2020). We also confirmed that the increase in *ORAI1* and *STIM1* transcription levels was paralleled by the respective increases in ORAI1 and STIM1 protein abundance, complementing the work of previous studies. Considering that ORAI1 and STIM1 in megakaryocytes is likely transferred into circulating platelets, SOCE is expected to be enhanced and thus sensitizes platelets to activators. Exaggerated platelet activation is strongly linked with thrombus formation, which accounts for the known high cardiovascular risk in patients with advanced CKD (Renga and Scavizzi, 2017).

4.3 Inhibitory effects of Mg^{2+} on Ca^{2+} signalling and SOCE

Hypomagnesemia is a common clinical complication in CKD patients and is inversely associated with cardiovascular and all-cause mortality (Wu et al., 2021, Ferre et al., 2018). However, the underlying mechanisms that drive the inverse association between Mg^{2+} and adverse cardiovascular outcomes have not been fully established. CsSRs are engaged in numerous physiological and pathological processes beyond their role in kidney function by precisely controlling Ca^{2+}

homeostasis in response to extracellular stimuli (Zhang et al., 2016). Mg^{2+}, a main ligand of CaSRs, interacts with the receptor and stimulates downstream signalling pathways. In VSMCs, Mg^{2+} can interfere with osteo/chondrogenic transformation and mitigate phosphate-induced vascular calcification upon CaSR activation. Additionally, Mg^{2+} and the CaSR agonist Gd^{3+} alleviate the stimulation of vascular calcification by phosphate via the inhibition of ORAI/STIM expression and SOCE activity. The presence of CaSR protein has previously been documented in both megakaryocytes and platelets (House et al., 1997). Moreover, CaSR activation has been reported to arrest the aggregation of platelets in hyperhomocysteinemia (Wang et al., 2017b).

Herein, we explored whether the β-glycerophosphate-triggered upregulation of NFAT5, SGK1, ORAI1, ORAI2, ORAI3, STIM1 and STIM2, as well as SOCE was reversed by 1.5 mM $MgCl_2$ and 50 μM of the CaSR agonist $GdCl_3$ in megakaryocytes, at least partially via the activation of CaSRs. Our present study does not, however, exclude the possibility that other signalling pathways may be involved in the reversal of β-glycerophosphate-stimulated enhancement of ORAI/STIM expression by Mg^{2+} in megakaryocytes. Of note is the fact that the signalling cascade shown in the present study is induced with a sustained incubation of Mg^{2+} or Gd^{3+}. Different signalling molecules may predominate after acute stimulation with Mg^{2+} or Gd^{3+}, such as through G protein-dependent activation of phospholipase C and inositol trisphosphate formation, as shown in other cell types (Zhang et al., 2019, Maltsev, 2018, Guo et al., 2021). In view of our current results and the functional role of CaSRs in the modulation of ORAI/STIM abundance, it can be inferred that Mg^{2+} supplementation has a protective influence on the suppression of platelet activation and thus lowers the risk for developing cardiac infarction and stroke in CKD patients.

Furthermore, the concentration of Mg^{2+} used in our study was 1.5 mM, a value

slightly above the reference range. Raising serum Mg^{2+} concentrations may be easily achieved by increasing the dialysate Mg^{2+} content in patients receiving haemodialysis or peritoneal dialysis and by increasing dietary Mg^{2+} intake or oral Mg^{2+} supplements in patients with non-dialysis CKD (Leenders et al., 2021). If the addition of Mg^{2+} indeed effectively decreases the occurrence of fatal and non-fatal cardiovascular events, it is likely to be an inexpensive intervention with a sufficiently high benefit-cost ratio. Nevertheless, additional experimental and clinical studies are required to determine the optimal therapeutic concentration in clinical practice.

4.4 Conclusion

In conclusion, $MgCl_2$ and $GdCl_3$ reverse the stimulatory impact of phosphate released from β-glycerophosphate on NFAT5, SGK1, ORAI and STIM isoforms as well as SOCE via the activation of CaSRs in megakaryocytes, suggesting that Mg^{2+} supplementation is a potentially useful therapeutic target to reduce cardiovascular risk in hyperphosphatemic patients with CKD. Further experiments are warranted to define the role of Mg^{2+} *in vivo* using relevant animal models.

5 Summary

Background: Impaired renal elimination of phosphate in chronic kidney disease (CKD) contributes to hyperphosphatemia, which in turn upregulates the expression of nuclear factor of activated T cells 5 (NFAT5) and serum and glucocorticoid-inducible kinase SGK1 (SGK1) in megakaryocytes and platelets. SGK1 is a potent stimulator of ORAI1, a Ca^{2+}-channel activated by Ca^{2+} sensor stromal interaction molecule 1 (STIM1) following the internal Ca^{2+} store depletion. Both ORAI1 and STIM1 are considered major components of store-operated Ca^{2+} entry (SOCE) and play a crucial role in platelet activation, thus accounting for the high risk for cardiovascular events in CKD patients. In vascular smooth muscle cells, sustained exposure to $MgCl_2$ and the Ca^{2+}-sensing receptor (CaSR) agonist $GdCl_3$ significantly attenuated the stimulatory effect of phosphate on ORAI1/STIM1 expression as well as SOCE activity. Our present study investigated whether phosphate-triggered upregulation of NFAT5, SGK1, ORAI1/2/3, STIM1/2 and SOCE is similarly sensitive to $MgCl_2$ or $GdCl_3$ in megakaryocytes. Methods: Human megakaryocytic cells (Meg-01) were exposed to 1.5 mM $MgCl_2$ or 50 µM $GdCl_3$ for 24 h without or with 2 mM β-glycerophosphate treatment. Transcript and protein abundance were evaluated utilizing qPCR and immunoblotting, respectively. Cytosolic Ca^{2+} activity was estimated by ratiometric Ca^{2+} imaging with Fura-2 fluorescence. SOCE activity was determined from the peak and slope of the increase in the 340/380 nm ratio, following extracellular Ca^{2+} re-addition after thapsigargin-evoked store depletion. Results: 1.5 mM $MgCl_2$ and 50 µM $GdCl_3$ upregulated CaSR expression and effectively reversed the phosphate-stimulated SOCE enhancement via inhibiting the signalling cascade of NFAT5/SGK1/ORAIs/STIMs. Conclusions: $MgCl_2$ and the CaSR agonist $GdCl_3$ are powerful regulators of ORAI1/STIM1 expression and SOCE, involved in phosphate-mediated Ca^{2+} signalling in megakaryocytes.

6 Zusammenfassung

Hintergrund: Eine gestörte renale Elimination von Phosphat bei der chronischen Nierenerkrankung (CKD) trägt zur Hyperphosphatämie bei, die wiederum die Hochregulierung der Expression des nukleären Faktors der aktivierten T-Zellen 5 (NFAT5) und der Serum- und Glukokortikoid-induzierbaren Kinase SGK1 (SGK1) in Megakaryozyten und Thrombozyten bedingt. SGK1 ist ein potenter Stimulator von ORAI1, einem Ca^{2+}-Kanal, der durch das Ca^{2+}-Sensor-Stroma-Interaktionsmolekül 1 (STIM1) nach der Erschöpfung des internen Ca^{2+}-Speichers aktiviert wird. Sowohl ORAI1 als auch STIM1 gelten als Hauptkomponenten des speichergesteuerten Ca^{2+}-Eintritts (SOCE) und spielen eine entscheidende Rolle bei der Thrombozytenaktivierung, wodurch das hohe Risiko kardiovaskulärer Ereignisse bei CKD-Patienten begründet wird. In glatten Gefäßmuskelzellen schwächte eine anhaltende Exposition gegenüber $MgCl_2$ und dem Ca^{2+}-erkennenden Rezeptor (CaSR)-Agonisten $GdCl_3$ die stimulierende Wirkung von Phosphat auf die ORAI1/STIM1-Expression, sowie die SOCE-Aktivität, signifikant ab. Unsere vorliegende Studie untersuchte, ob die durch Phosphat ausgelöste Hochregulation von NFAT5, SGK1, ORAI1/2/3, STIM1/2 und SOCE in Megakaryozyten ähnlich sensitiv gegenüber $MgCl_2$ oder $GdCl_3$ ist. Methoden: Humane Megakaryozytenzellen (Meg-01) wurden ohne oder mit 2 mM β-Glycerophosphat-Behandlung für 24 h 1,5 mM $MgCl_2$ oder 50 µM $GdCl_3$ ausgesetzt. Transkript und Proteingehalt wurden mittels qPCR bzw. Immunoblot bewertet. Die zytosolische Ca^{2+}-Aktivität wurde mit Hilfe eines Fura-2-Fluoreszenz-Ansatzes abgeschätzt. Die SOCE-Aktivität wurde nach einer durch Thapsigargin herbeigeführten Speicherdepletion anschließend bei erneuter extrazellulärer Ca^{2+}-Zugabe aus dem Höhepunkt und der Steigung des Anstiegs des 340/380-nm-Verhältnisses bestimmt. Ergebnisse: 1,5 mM $MgCl_2$ und 50 µM $GdCl_3$ regulierten die CaSR-Expression hoch und kehrten die Phosphat-

stimulierte SOCE-Verstärkung durch Hemmung der Signalkaskade von NFAT5/SGK1/ORAIs/STIMs effektiv um. Schlussfolgerungen: $MgCl_2$ und der CaSR-Agonist $GdCl_3$ sind starke Regulatoren der ORAI1/STIM1-Expression und SOCE, die an der Phosphat-vermittelten Ca^{2+}-Signalgebung in Megakaryozyten beteiligt sind.

7 Bibliography

AHMAD, F., BOULAFTALI, Y., GREENE, T. K., OUELLETTE, T. D., PONCZ, M., FESKE, S. & BERGMEIER, W. 2011. Relative contributions of stromal interaction molecule 1 and CalDAG-GEFI to calcium-dependent platelet activation and thrombosis. *J Thromb Haemost,* 9**,** 2077-86.

ALESUTAN, I., TUFFAHA, R., AUER, T., FEGER, M., PIESKE, B., LANG, F. & VOELKL, J. 2017. Inhibition of osteo/chondrogenic transformation of vascular smooth muscle cells by MgCl2 via calcium-sensing receptor. *J Hypertens,* 35**,** 523-532.

ANAVEKAR, N. S., MCMURRAY, J. J., VELAZQUEZ, E. J., SOLOMON, S. D., KOBER, L., ROULEAU, J. L., WHITE, H. D., NORDLANDER, R., MAGGIONI, A., DICKSTEIN, K., ZELENKOFSKE, S., LEIMBERGER, J. D., CALIFF, R. M. & PFEFFER, M. A. 2004. Relation between renal dysfunction and cardiovascular outcomes after myocardial infarction. *N Engl J Med,* 351**,** 1285-95.

ANDO, M., IWATA, A., OZEKI, Y., TSUCHIYA, K., AKIBA, T. & NIHEI, H. 2002. Circulating platelet-derived microparticles with procoagulant activity may be a potential cause of thrombosis in uremic patients. *Kidney Int,* 62**,** 1757-63.

BAATEN, C., STERNKOPF, M., HENNING, T., MARX, N., JANKOWSKI, J. & NOELS, H. 2021. Platelet Function in CKD: A Systematic Review and Meta-Analysis. *J Am Soc Nephrol,* 32**,** 1583-1598.

BABA, Y., HAYASHI, K., FUJII, Y., MIZUSHIMA, A., WATARAI, H., WAKAMORI, M., NUMAGA, T., MORI, Y., IINO, M., HIKIDA, M. & KUROSAKI, T. 2006. Coupling of STIM1 to store-operated Ca2+ entry through its constitutive and inducible movement in the endoplasmic reticulum. *Proc Natl Acad Sci U S A,* 103**,** 16704-9.

BERGMEIER, W., OH-HORA, M., MCCARL, C. A., RODEN, R. C., BRAY, P. F. & FESKE, S. 2009. R93W mutation in Orai1 causes impaired calcium influx in platelets. *Blood,* 113**,** 675-8.

BERNA-ERRO, A., JARDIN, I., SMANI, T. & ROSADO, J. A. 2016. Regulation of Platelet Function by Orai, STIM and TRP. *Adv Exp Med Biol,* 898**,** 157-81.

BERNA-ERRO, A., REDONDO, P. C. & ROSADO, J. A. 2012. Store-operated Ca(2+) entry. *Adv Exp Med Biol,* 740**,** 349-82.

BEVERS, E. M., COMFURIUS, P. & ZWAAL, R. F. 1991. Platelet procoagulant activity: physiological significance and mechanisms of exposure. *Blood Rev,* 5**,** 146-54.

BHARDWAJ, R., HEDIGER, M. A. & DEMAUREX, N. 2016. Redox modulation of STIM-ORAI signaling. *Cell Calcium,* 60**,** 142-52.

BLACHER, J., GUERIN, A. P., PANNIER, B., MARCHAIS, S. J. & LONDON, G. M. 2001. Arterial calcifications, arterial stiffness, and cardiovascular risk in end-stage renal disease. *Hypertension,* 38**,** 938-42.

BONOMINI, M., DOTTORI, S., AMOROSO, L., ARDUINI, A. & SIROLLI, V. 2004. Increased platelet phosphatidylserine exposure and caspase activation in chronic uremia. *J Thromb Haemost,* 2**,** 1275-81.

BONOMINI, M., SIROLLI, V., DOTTORI, S., AMOROSO, L., DI LIBERATO, L. & ARDUINI, A. 2007. L-carnitine inhibits a subset of platelet activation responses in chronic uraemia. *Nephrol Dial Transplant,* 22**,** 2623-9.

BOOTMAN, M. D., LIPP, P. & BERRIDGE, M. J. 2001. The organisation and functions of local Ca(2+) signals. *J Cell Sci,* 114**,** 2213-22.

BORST, O., SCHMIDT, E. M., MUNZER, P., SCHONBERGER, T., TOWHID, S. T., ELVERS, M., LEIBROCK, C., SCHMID, E., EYLENSTEIN, A., KUHL, D., MAY, A. E., GAWAZ, M. & LANG, F. 2012. The serum- and glucocorticoid-inducible kinase 1 (SGK1) influences platelet calcium signaling and function by regulation of Orai1 expression in megakaryocytes. *Blood,* 119**,** 251-61.

BRANDMAN, O., LIOU, J., PARK, W. S. & MEYER, T. 2007. STIM2 is a feedback regulator that stabilizes basal cytosolic and endoplasmic reticulum Ca2+ levels. *Cell,* 131**,** 1327-39.

BRAUN, A., VARGA-SZABO, D., KLEINSCHNITZ, C., PLEINES, I., BENDER, M., AUSTINAT, M., BOSL, M., STOLL, G. & NIESWANDT, B. 2009. Orai1 (CRACM1) is the platelet SOC channel and essential for pathological thrombus formation. *Blood,* 113**,** 2056-63.

BRAUN, A., VOGTLE, T., VARGA-SZABO, D. & NIESWANDT, B. 2011. STIM and Orai in hemostasis and thrombosis. *Front Biosci (Landmark Ed),* 16**,** 2144-60.

BRENNAN, S. C., THIEM, U., ROTH, S., AGGARWAL, A., FETAHU, I., TENNAKOON, S., GOMES, A. R., BRANDI, M. L., BRUGGEMAN, F., MENTAVERRI, R., RICCARDI, D. & KALLAY, E. 2013. Calcium sensing receptor signalling in physiology and cancer. *Biochim Biophys Acta,* 1833**,** 1732-44.

BRESSENDORFF, I., HANSEN, D., SCHOU, M., PASCH, A. & BRANDI, L. 2018. The Effect of Increasing Dialysate Magnesium on Serum Calcification Propensity in Subjects with End Stage Kidney Disease: A Randomized, Controlled Clinical Trial. *Clin J Am Soc Nephrol,* 13**,** 1373-1380.

BRESSENDORFF, I., HANSEN, D., SCHOU, M., SILVER, B., PASCH, A., BOUCHELOUCHE, P., PEDERSEN, L., RASMUSSEN, L. M. & BRANDI, L. 2017. Oral Magnesium Supplementation in Chronic Kidney Disease Stages 3 and 4: Efficacy, Safety, and Effect on Serum Calcification

Propensity-A Prospective Randomized Double-Blinded Placebo-Controlled Clinical Trial. *Kidney Int Rep, 2*, 380-389.

CAHALAN, M. D. 2009. STIMulating store-operated Ca(2+) entry. *Nat Cell Biol,* 11, 669-77.

CHANG, W., TU, C., CHEN, T. H., KOMUVES, L., ODA, Y., PRATT, S. A., MILLER, S. & SHOBACK, D. 1999. Expression and signal transduction of calcium-sensing receptors in cartilage and bone. *Endocrinology,* 140, 5883-93.

CHATTOPADHYAY, N., CHENG, I., ROGERS, K., RICCARDI, D., HALL, A., DIAZ, R., HEBERT, S. C., SOYBEL, D. I. & BROWN, E. M. 1998. Identification and localization of extracellular Ca(2+)-sensing receptor in rat intestine. *Am J Physiol,* 274, G122-30.

CHEN, S., GRIGSBY, C. L., LAW, C. S., NI, X., NEKREP, N., OLSEN, K., HUMPHREYS, M. H. & GARDNER, D. G. 2009. Tonicity-dependent induction of Sgk1 expression has a potential role in dehydration-induced natriuresis in rodents. *J Clin Invest,* 119, 1647-58.

CHEUNG, C. Y. & KO, B. C. 2013. NFAT5 in cellular adaptation to hypertonic stress - regulations and functional significance. *J Mol Signal,* 8, 5.

CHRONIC KIDNEY DISEASE PROGNOSIS, C., MATSUSHITA, K., VAN DER VELDE, M., ASTOR, B. C., WOODWARD, M., LEVEY, A. S., DE JONG, P. E., CORESH, J. & GANSEVOORT, R. T. 2010. Association of estimated glomerular filtration rate and albuminuria with all-cause and cardiovascular mortality in general population cohorts: a collaborative meta-analysis. *Lancet,* 375, 2073-81.

COBURN, J. W., ELANGOVAN, L., GOODMAN, W. G. & FRAZAO, J. M. 1999. Calcium-sensing receptor and calcimimetic agents. *Kidney Int Suppl,* 73, S52-8.

CONIGRAVE, A. D. & WARD, D. T. 2013. Calcium-sensing receptor (CaSR): pharmacological properties and signaling pathways. *Best Pract Res Clin Endocrinol Metab,* 27, 315-31.

DERLER, I., JARDIN, I. & ROMANIN, C. 2016. Molecular mechanisms of STIM/Orai communication. *Am J Physiol Cell Physiol,* 310, C643-62.

DI BUDUO, C. A., BALDUINI, A. & MOCCIA, F. 2016. Pathophysiological Significance of Store-Operated Calcium Entry in Megakaryocyte Function: Opening New Paths for Understanding the Role of Calcium in Thrombopoiesis. *Int J Mol Sci,* 17, 2055.

DIAZ-SOTO, G., ROCHER, A., GARCIA-RODRIGUEZ, C., NUNEZ, L. & VILLALOBOS, C. 2016. The Calcium-Sensing Receptor in Health and Disease. *Int Rev Cell Mol Biol,* 327, 321-369.

EDWARDS, N. C., STEEDS, R. P., FERRO, C. J. & TOWNEND, J. N. 2006. The treatment of coronary artery disease in patients with chronic kidney

disease. *QJM,* 99**,** 723-36.

ERCAN, E., CHUNG, S. H., BHARDWAJ, R. & SEEDORF, M. 2012. Di-arginine signals and the K-rich domain retain the Ca(2)(+) sensor STIM1 in the endoplasmic reticulum. *Traffic,* 13**,** 992-1003.

EYLENSTEIN, A., GEHRING, E. M., HEISE, N., SHUMILINA, E., SCHMIDT, S., SZTEYN, K., MUNZER, P., NURBAEVA, M. K., EICHENMULLER, M., TYAN, L., REGEL, I., FOLLER, M., KUHL, D., SOBOLOFF, J., PENNER, R. & LANG, F. 2011. Stimulation of Ca2+-channel Orai1/STIM1 by serum- and glucocorticoid-inducible kinase 1 (SGK1). *FASEB J,* 25**,** 2012-21.

FAHRNER, M., MUIK, M., SCHINDL, R., BUTORAC, C., STATHOPULOS, P., ZHENG, L., JARDIN, I., IKURA, M. & ROMANIN, C. 2014. A coiled-coil clamp controls both conformation and clustering of stromal interaction molecule 1 (STIM1). *J Biol Chem,* 289**,** 33231-44.

FAHRNER, M., SCHINDL, R., MUIK, M., DERLER, I. & ROMANIN, C. 2017. The STIM-Orai Pathway: The Interactions Between STIM and Orai. *Adv Exp Med Biol,* 993**,** 59-81.

FAHRNER, M., SCHINDL, R. & ROMANIN, C. 2018. Studies of Structure-Function and Subunit Composition of Orai/STIM Channel. *In:* KOZAK, J. A. & PUTNEY, J. W., JR. (eds.) *Calcium Entry Channels in Non-Excitable Cells.* Boca Raton (FL).

FERRE, S., LI, X., ADAMS-HUET, B., MAALOUF, N. M., SAKHAEE, K., TOTO, R. D., MOE, O. W. & NEYRA, J. A. 2018. Association of serum magnesium with all-cause mortality in patients with and without chronic kidney disease in the Dallas Heart Study. *Nephrol Dial Transplant,* 33**,** 1389-1396.

FRISCHAUF, I., FAHRNER, M., JARDIN, I. & ROMANIN, C. 2016. The STIM1: Orai Interaction. *Adv Exp Med Biol,* 898**,** 25-46.

FRISCHAUF, I., MUIK, M., DERLER, I., BERGSMANN, J., FAHRNER, M., SCHINDL, R., GROSCHNER, K. & ROMANIN, C. 2009. Molecular determinants of the coupling between STIM1 and Orai channels: differential activation of Orai1-3 channels by a STIM1 coiled-coil mutant. *J Biol Chem,* 284**,** 21696-706.

FRISCHAUF, I., SCHINDL, R., BERGSMANN, J., DERLER, I., FAHRNER, M., MUIK, M., FRITSCH, R., LACKNER, B., GROSCHNER, K. & ROMANIN, C. 2011. Cooperativeness of Orai cytosolic domains tunes subtype-specific gating. *J Biol Chem,* 286**,** 8577-8584.

FURIE, B., FURIE, B. C. & FLAUMENHAFT, R. 2001. A journey with platelet P-selectin: the molecular basis of granule secretion, signalling and cell adhesion. *Thromb Haemost,* 86**,** 214-21.

GARRAUD, O. & COGNASSE, F. 2015. Are Platelets Cells? And if Yes, are

They Immune Cells? *Front Immunol,* 6**,** 70.

GAWAZ, M., LANGER, H. & MAY, A. E. 2005. Platelets in inflammation and atherogenesis. *J Clin Invest,* 115**,** 3378-84.

GERBINO, A. & COLELLA, M. 2018. The Different Facets of Extracellular Calcium Sensors: Old and New Concepts in Calcium-Sensing Receptor Signalling and Pharmacology. *Int J Mol Sci,* 19.

GILIO, K., VAN KRUCHTEN, R., BRAUN, A., BERNA-ERRO, A., FEIJGE, M. A., STEGNER, D., VAN DER MEIJDEN, P. E., KUIJPERS, M. J., VARGA-SZABO, D., HEEMSKERK, J. W. & NIESWANDT, B. 2010. Roles of platelet STIM1 and Orai1 in glycoprotein VI- and thrombin-dependent procoagulant activity and thrombus formation. *J Biol Chem,* 285**,** 23629-38.

GOLFIER, S., KONDO, S., SCHULZE, T., TAKEUCHI, T., VASSILEVA, G., ACHTMAN, A. H., GRALER, M. H., ABBONDANZO, S. J., WIEKOWSKI, M., KREMMER, E., ENDO, Y., LIRA, S. A., BACON, K. B. & LIPP, M. 2010. Shaping of terminal megakaryocyte differentiation and proplatelet development by sphingosine-1-phosphate receptor S1P4. *FASEB J,* 24**,** 4701-10.

GRABMAYR, H., ROMANIN, C. & FAHRNER, M. 2020. STIM Proteins: An Ever-Expanding Family. *Int J Mol Sci,* 22.

GROBER, U., SCHMIDT, J. & KISTERS, K. 2015. Magnesium in Prevention and Therapy. *Nutrients,* 7**,** 8199-226.

GUO, R. W. & HUANG, L. 2008. New insights into the activation mechanism of store-operated calcium channels: roles of STIM and Orai. *J Zhejiang Univ Sci B,* 9**,** 591-601.

GUO, S., YAN, T., SHI, L., LIU, A., ZHANG, T., XU, Y., JIANG, W., YANG, Q., YANG, L., LIU, L., ZHAO, R. & ZHANG, S. 2021. Matrine, as a CaSR agonist promotes intestinal GLP-1 secretion and improves insulin resistance in diabetes mellitus. *Phytomedicine,* 84**,** 153507.

HAMADA, T., MOHLE, R., HESSELGESSER, J., HOXIE, J., NACHMAN, R. L., MOORE, M. A. & RAFII, S. 1998. Transendothelial migration of megakaryocytes in response to stromal cell-derived factor 1 (SDF-1) enhances platelet formation. *J Exp Med,* 188**,** 539-48.

HERNANDEZ-OCHOA, E. O., ROBISON, P., CONTRERAS, M., SHEN, T., ZHAO, Z. & SCHNEIDER, M. F. 2012. Elevated extracellular glucose and uncontrolled type 1 diabetes enhance NFAT5 signaling and disrupt the transverse tubular network in mouse skeletal muscle. *Exp Biol Med (Maywood),* 237**,** 1068-83.

HEWAVITHARANA, T., DENG, X., SOBOLOFF, J. & GILL, D. L. 2007. Role of STIM and Orai proteins in the store-operated calcium signaling pathway. *Cell Calcium,* 42**,** 173-82.

HOTH, M. & NIEMEYER, B. A. 2013. The neglected CRAC proteins: Orai2, Orai3, and STIM2. *Curr Top Membr,* 71**,** 237-71.

HOUSE, M. G., KOHLMEIER, L., CHATTOPADHYAY, N., KIFOR, O., YAMAGUCHI, T., LEBOFF, M. S., GLOWACKI, J. & BROWN, E. M. 1997. Expression of an extracellular calcium-sensing receptor in human and mouse bone marrow cells. *J Bone Miner Res,* 12**,** 1959-70.

HRUSKA, K. A., MATHEW, S., LUND, R., QIU, P. & PRATT, R. 2008. Hyperphosphatemia of chronic kidney disease. *Kidney Int,* 74**,** 148-57.

ITALIANO, J. E., JR., LECINE, P., SHIVDASANI, R. A. & HARTWIG, J. H. 1999. Blood platelets are assembled principally at the ends of proplatelet processes produced by differentiated megakaryocytes. *J Cell Biol,* 147**,** 1299-312.

ITALIANO, J. E., JR. & SHIVDASANI, R. A. 2003. Megakaryocytes and beyond: the birth of platelets. *J Thromb Haemost,* 1**,** 1174-82.

JOHNSON, M. 2019. Calcium Imaging of Store-Operated Calcium (Ca(2+)) Entry (SOCE) in HEK293 Cells Using Fura-2. *Methods Mol Biol,* 1925**,** 163-172.

JOHNSTONE, L. S., GRAHAM, S. J. & DZIADEK, M. A. 2010. STIM proteins: integrators of signalling pathways in development, differentiation and disease. *J Cell Mol Med,* 14**,** 1890-903.

KAESLER, N., GOETTSCH, C., WEIS, D., SCHURGERS, L., HELLMANN, B., FLOEGE, J. & KRAMANN, R. 2020. Magnesium but not nicotinamide prevents vascular calcification in experimental uraemia. *Nephrol Dial Transplant,* 35**,** 65-73.

KARBOWSKA, M., KAMINSKI, T. W., MARCINCZYK, N., MISZTAL, T., RUSAK, T., SMYK, L. & PAWLAK, D. 2017. The Uremic Toxin Indoxyl Sulfate Accelerates Thrombotic Response after Vascular Injury in Animal Models. *Toxins (Basel),* 9**,** 229.

KAUFMAN, R. M., AIRO, R., POLLACK, S. & CROSBY, W. H. 1965. Circulating megakaryocytes and platelet release in the lung. *Blood,* 26**,** 720-31.

KAUSHANSKY, K. 2015. Thrombopoiesis. *Semin Hematol,* 52**,** 4-11.

KAWASAKI, T., LANGE, I. & FESKE, S. 2009. A minimal regulatory domain in the C terminus of STIM1 binds to and activates ORAI1 CRAC channels. *Biochem Biophys Res Commun,* 385**,** 49-54.

KROTZ, F., SOHN, H. Y. & POHL, U. 2004. Reactive oxygen species: players in the platelet game. *Arterioscler Thromb Vasc Biol,* 24**,** 1988-96.

LANG, F., BOHMER, C., PALMADA, M., SEEBOHM, G., STRUTZ-SEEBOHM, N. & VALLON, V. 2006. (Patho)physiological significance of the serum- and glucocorticoid-inducible kinase isoforms. *Physiol Rev,* 86**,** 1151-78.

LANG, F., GAWAZ, M. & BORST, O. 2015. The serum- & glucocorticoid-inducible kinase in the regulation of platelet function. *Acta Physiol (Oxf),*

213**,** 181-90.

LANG, F., GUELINCKX, I., LEMETAIS, G. & MELANDER, O. 2017. Two Liters a Day Keep the Doctor Away? Considerations on the Pathophysiology of Suboptimal Fluid Intake in the Common Population. *Kidney Blood Press Res,* 42**,** 483-494.

LANG, F., MUNZER, P., GAWAZ, M. & BORST, O. 2013. Regulation of STIM1/Orai1-dependent Ca2+ signalling in platelets. *Thromb Haemost,* 110**,** 925-30.

LANG, F., PELZL, L., HAUSER, S., HERMANN, A., STOURNARAS, C. & SCHOLS, L. 2018. To die or not to die SGK1-sensitive ORAI/STIM in cell survival. *Cell Calcium,* 74**,** 29-34.

LANG, F. & SHUMILINA, E. 2013. Regulation of ion channels by the serum- and glucocorticoid-inducible kinase SGK1. *FASEB J,* 27**,** 3-12.

LANG, F. & VOELKL, J. 2013. Therapeutic potential of serum and glucocorticoid inducible kinase inhibition. *Expert Opin Investig Drugs,* 22**,** 701-14.

LEENDERS, N. H. J., VERMEULEN, E. A., VAN BALLEGOOIJEN, A. J., HOEKSTRA, T., DE VRIES, R., BEULENS, J. W. & VERVLOET, M. G. 2021. The association between circulating magnesium and clinically relevant outcomes in patients with chronic kidney disease: A systematic review and meta-analysis. *Clin Nutr,* 40**,** 3133-3147.

LEIBROCK, C. B., ALESUTAN, I., VOELKL, J., PAKLADOK, T., MICHAEL, D., SCHLEICHER, E., KAMYABI-MOGHADDAM, Z., QUINTANILLA-MARTINEZ, L., KURO-O, M. & LANG, F. 2015. NH4Cl Treatment Prevents Tissue Calcification in Klotho Deficiency. *J Am Soc Nephrol,* 26**,** 2423-33.

LEWIS, R. S. 2011. Store-operated calcium channels: new perspectives on mechanism and function. *Cold Spring Harb Perspect Biol,* 3**,** a003970.

LIS, A., ZIERLER, S., PEINELT, C., FLEIG, A. & PENNER, R. 2010. A single lysine in the N-terminal region of store-operated channels is critical for STIM1-mediated gating. *J Gen Physiol,* 136**,** 673-86.

LUIK, R. M., WANG, B., PRAKRIYA, M., WU, M. M. & LEWIS, R. S. 2008. Oligomerization of STIM1 couples ER calcium depletion to CRAC channel activation. *Nature,* 454**,** 538-42.

LUIK, R. M., WU, M. M., BUCHANAN, J. & LEWIS, R. S. 2006. The elementary unit of store-operated Ca2+ entry: local activation of CRAC channels by STIM1 at ER-plasma membrane junctions. *J Cell Biol,* 174**,** 815-25.

LUTZ, J., MENKE, J., SOLLINGER, D., SCHINZEL, H. & THURMEL, K. 2014. Haemostasis in chronic kidney disease. *Nephrol Dial Transplant,* 29**,** 29-40.

LUTZ, P. & JURK, P. 2020. Platelets in Advanced Chronic Kidney Disease: Two Sides of the Coin. *Semin Thromb Hemost,* 46**,** 342-356.

MA, K., LIU, P., AL-MAGHOUT, T., SUKKAR, B., CAO, H., VOELKL, J., ALESUTAN, I., PIESKE, B. & LANG, F. 2019. Phosphate-induced ORAI1 expression and store-operated Ca(2+) entry in aortic smooth muscle cells. *J Mol Med (Berl),* 97**,** 1465-1475.

MACHLUS, K. R. & ITALIANO, J. E., JR. 2013. The incredible journey: From megakaryocyte development to platelet formation. *J Cell Biol,* 201**,** 785-96.

MALTSEV, A. V. 2018. Agmatine modulates calcium handling in cardiomyocytes of hibernating ground squirrels through calcium-sensing receptor signaling. *Cell Signal,* 51**,** 1-12.

MANJI, S. S., PARKER, N. J., WILLIAMS, R. T., VAN STEKELENBURG, L., PEARSON, R. B., DZIADEK, M. & SMITH, P. J. 2000. STIM1: a novel phosphoprotein located at the cell surface. *Biochim Biophys Acta,* 1481**,** 147-55.

MANN, J. F., GERSTEIN, H. C., POGUE, J., BOSCH, J. & YUSUF, S. 2001. Renal insufficiency as a predictor of cardiovascular outcomes and the impact of ramipril: the HOPE randomized trial. *Ann Intern Med,* 134**,** 629-36.

MASSY, Z. A. & DRUEKE, T. B. 2012. Magnesium and outcomes in patients with chronic kidney disease: focus on vascular calcification, atherosclerosis and survival. *Clin Kidney J,* 5**,** i52-i61.

MATSUO, T., KOIDE, M., KARIO, K., SUZUKI, S. & MATSUO, M. 1997. Extrinsic coagulation factors and tissue factor pathway inhibitor in end-stage chronic renal failure. *Haemostasis,* 27**,** 163-7.

MAY, A. E., LANGER, H., SEIZER, P., BIGALKE, B., LINDEMANN, S. & GAWAZ, M. 2007. Platelet-leukocyte interactions in inflammation and atherothrombosis. *Semin Thromb Hemost,* 33**,** 123-7.

MAY, A. E., SEIZER, P. & GAWAZ, M. 2008. Platelets: inflammatory firebugs of vascular walls. *Arterioscler Thromb Vasc Biol,* 28**,** s5-10.

MERCER, J. C., DEHAVEN, W. I., SMYTH, J. T., WEDEL, B., BOYLES, R. R., BIRD, G. S. & PUTNEY, J. W., JR. 2006. Large store-operated calcium selective currents due to co-expression of Orai1 or Orai2 with the intracellular calcium sensor, Stim1. *J Biol Chem,* 281**,** 24979-90.

MIZOBUCHI, M., TOWLER, D. & SLATOPOLSKY, E. 2009. Vascular calcification: the killer of patients with chronic kidney disease. *J Am Soc Nephrol,* 20**,** 1453-64.

MOLINO, D., DE LUCIA, D. & GASPARE DE SANTO, N. 2006. Coagulation disorders in uremia. *Semin Nephrol,* 26**,** 46-51.

MORADI, H., SICA, D. A. & KALANTAR-ZADEH, K. 2013. Cardiovascular burden associated with uremic toxins in patients with chronic kidney disease. *Am J Nephrol,* 38**,** 136-48.

MORTAZAVI, M., MOEINZADEH, F., SAADATNIA, M., SHAHIDI, S., MCGEE, J. C. & MINAGAR, A. 2013. Effect of magnesium supplementation on carotid intima-media thickness and flow-mediated dilatation among hemodialysis patients: a double-blind, randomized, placebo-controlled trial. *Eur Neurol,* 69**,** 309-16.

MOTIANI, R. K., STOLWIJK, J. A., NEWTON, R. L., ZHANG, X. & TREBAK, M. 2013. Emerging roles of Orai3 in pathophysiology. *Channels (Austin),* 7**,** 392-401.

MUIK, M., FAHRNER, M., DERLER, I., SCHINDL, R., BERGSMANN, J., FRISCHAUF, I., GROSCHNER, K. & ROMANIN, C. 2009. A Cytosolic Homomerization and a Modulatory Domain within STIM1 C Terminus Determine Coupling to ORAI1 Channels. *J Biol Chem,* 284**,** 8421-6.

MUIK, M., FRISCHAUF, I., DERLER, I., FAHRNER, M., BERGSMANN, J., EDER, P., SCHINDL, R., HESCH, C., POLZINGER, B., FRITSCH, R., KAHR, H., MADL, J., GRUBER, H., GROSCHNER, K. & ROMANIN, C. 2008. Dynamic coupling of the putative coiled-coil domain of ORAI1 with STIM1 mediates ORAI1 channel activation. *J Biol Chem,* 283**,** 8014-22.

NASSA, G., GIURATO, G., CIMMINO, G., RIZZO, F., RAVO, M., SALVATI, A., NYMAN, T. A., ZHU, Y., VESTERLUND, M., LEHTIO, J., GOLINO, P., WEISZ, A. & TARALLO, R. 2018. Splicing of platelet resident pre-mRNAs upon activation by physiological stimuli results in functionally relevant proteome modifications. *Sci Rep,* 8**,** 498.

NAVARRO-BORELLY, L., SOMASUNDARAM, A., YAMASHITA, M., REN, D., MILLER, R. J. & PRAKRIYA, M. 2008. STIM1-Orai1 interactions and Orai1 conformational changes revealed by live-cell FRET microscopy. *J Physiol,* 586**,** 5383-401.

NEUHOFER, W. 2010. Role of NFAT5 in inflammatory disorders associated with osmotic stress. *Curr Genomics,* 11**,** 584-90.

NGUYEN, N. T., HAN, W., CAO, W. M., WANG, Y., WEN, S., HUANG, Y., LI, M., DU, L. & ZHOU, Y. 2018. Store-Operated Calcium Entry Mediated by ORAI and STIM. *Compr Physiol,* 8**,** 981-1002.

NIESWANDT, B. & WATSON, S. P. 2003. Platelet-collagen interaction: is GPVI the central receptor? *Blood,* 102**,** 449-61.

OGURA, M., MORISHIMA, Y., OHNO, R., KATO, Y., HIRABAYASHI, N., NAGURA, H. & SAITO, H. 1985. Establishment of a novel human megakaryoblastic leukemia cell line, MEG-01, with positive Philadelphia chromosome. *Blood,* 66**,** 1384-92.

PARK, C. Y., HOOVER, P. J., MULLINS, F. M., BACHHAWAT, P., COVINGTON, E. D., RAUNSER, S., WALZ, T., GARCIA, K. C., DOLMETSCH, R. E. & LEWIS, R. S. 2009. STIM1 clusters and activates CRAC channels via direct binding of a cytosolic domain to Orai1. *Cell,* 136**,** 876-90.

PATEL, S. R., HARTWIG, J. H. & ITALIANO, J. E., JR. 2005. The biogenesis of platelets from megakaryocyte proplatelets. *J Clin Invest,* 115**,** 3348-54.

PEINELT, C., VIG, M., KOOMOA, D. L., BECK, A., NADLER, M. J., KOBLAN-HUBERSON, M., LIS, A., FLEIG, A., PENNER, R. & KINET, J. P. 2006. Amplification of CRAC current by STIM1 and CRACM1 (Orai1). *Nat Cell Biol,* 8**,** 771-3.

PELZL, L., SAHU, I., MA, K., HEINZMANN, D., BHUYAN, A. A. M., AL-MAGHOUT, T., SUKKAR, B., SHARMA, Y., MARINI, I., RIGONI, F., ARTUNC, F., CAO, H., GUTTI, R., VOELKL, J., PIESKE, B., GAWAZ, M., BAKCHOUL, T. & LANG, F. 2020. Beta-Glycerophosphate-Induced ORAI1 Expression and Store Operated Ca(2+) Entry in Megakaryocytes. *Sci Rep,* 10**,** 1728.

POTIER, M. & TREBAK, M. 2008. New developments in the signaling mechanisms of the store-operated calcium entry pathway. *Pflugers Arch,* 457**,** 405-15.

PRAKRIYA, M. 2013. Store-operated Orai channels: structure and function. *Curr Top Membr,* 71**,** 1-32.

PRAKRIYA, M. & LEWIS, R. S. 2015. Store-Operated Calcium Channels. *Physiol Rev,* 95**,** 1383-436.

RENGA, B. & SCAVIZZI, F. 2017. Platelets and cardiovascular risk. *Acta Cardiol,* 72**,** 2-8.

RICCARDI, D., PARK, J., LEE, W. S., GAMBA, G., BROWN, E. M. & HEBERT, S. C. 1995. Cloning and functional expression of a rat kidney extracellular calcium/polyvalent cation-sensing receptor. *Proc Natl Acad Sci U S A,* 92**,** 131-5.

RODRIGUEZ-ORTIZ, M. E., CANALEJO, A., HERENCIA, C., MARTINEZ-MORENO, J. M., PERALTA-RAMIREZ, A., PEREZ-MARTINEZ, P., NAVARRO-GONZALEZ, J. F., RODRIGUEZ, M., PETER, M., GUNDLACH, K., STEPPAN, S., PASSLICK-DEETJEN, J., MUNOZ-CASTANEDA, J. R. & ALMADEN, Y. 2014. Magnesium modulates parathyroid hormone secretion and upregulates parathyroid receptor expression at moderately low calcium concentration. *Nephrol Dial Transplant,* 29**,** 282-9.

SAHU, I., PELZL, L., SUKKAR, B., FAKHRI, H., AL-MAGHOUT, T., CAO, H., HAUSER, S., GUTTI, R., GAWAZ, M. & LANG, F. 2017. NFAT5-sensitive Orai1 expression and store-operated Ca(2+) entry in megakaryocytes. *FASEB J,* 31**,** 3439-3448.

SAITOH, N., ORITANI, K., SAITO, K., YOKOTA, T., ICHII, M., SUDO, T., FUJITA, N., NAKAJIMA, K., OKADA, M. & KANAKURA, Y. 2011. Identification of functional domains and novel binding partners of STIM proteins. *J Cell Biochem,* 112**,** 147-56.

SCHIFFRIN, E. L., LIPMAN, M. L. & MANN, J. F. 2007. Chronic kidney disease: effects on the cardiovascular system. *Circulation,* 116**,** 85-97.

SCHULTZ, J., PONTING, C. P., HOFMANN, K. & BORK, P. 1997. SAM as a protein interaction domain involved in developmental regulation. *Protein Sci,* 6**,** 249-53.

SEO, J. W. & PARK, T. J. 2008. Magnesium metabolism. *Electrolyte Blood Press,* 6**,** 86-95.

SHIM, A. H., TIRADO-LEE, L. & PRAKRIYA, M. 2015. Structural and functional mechanisms of CRAC channel regulation. *J Mol Biol,* 427**,** 77-93.

SIROLLI, V., STRIZZI, L., DI STANTE, S., ROBUFFO, I., PROCOPIO, A. & BONOMINI, M. 2001. Platelet activation and platelet-erythrocyte aggregates in end-stage renal disease patients on hemodialysis. *Thromb Haemost,* 86**,** 834-9.

SOBOLOFF, J., ROTHBERG, B. S., MADESH, M. & GILL, D. L. 2012. STIM proteins: dynamic calcium signal transducers. *Nat Rev Mol Cell Biol,* 13**,** 549-65.

SOBOLOFF, J., SPASSOVA, M. A., HEWAVITHARANA, T., HE, L. P., XU, W., JOHNSTONE, L. S., DZIADEK, M. A. & GILL, D. L. 2006. STIM2 is an inhibitor of STIM1-mediated store-operated Ca2+ Entry. *Curr Biol,* 16**,** 1465-70.

STATHOPULOS, P. B. & IKURA, M. 2010. Partial unfolding and oligomerization of stromal interaction molecules as an initiation mechanism of store operated calcium entry. *Biochem Cell Biol,* 88**,** 175-83.

STATHOPULOS, P. B., LI, G. Y., PLEVIN, M. J., AMES, J. B. & IKURA, M. 2006. Stored Ca2+ depletion-induced oligomerization of stromal interaction molecule 1 (STIM1) via the EF-SAM region: An initiation mechanism for capacitive Ca2+ entry. *J Biol Chem,* 281**,** 35855-62.

STATHOPULOS, P. B., ZHENG, L., LI, G. Y., PLEVIN, M. J. & IKURA, M. 2008. Structural and mechanistic insights into STIM1-mediated initiation of store-operated calcium entry. *Cell,* 135**,** 110-22.

SWAMINATHAN, R. 2003. Magnesium metabolism and its disorders. *Clin Biochem Rev,* 24**,** 47-66.

TAKAHASHI, Y., MURAKAMI, M., WATANABE, H., HASEGAWA, H., OHBA, T., MUNEHISA, Y., NOBORI, K., ONO, K., IIJIMA, T. & ITO, H. 2007. Essential role of the N-terminus of murine Orai1 in store-operated Ca2+ entry. *Biochem Biophys Res Commun,* 356**,** 45-52.

TAKEUCHI, K., SATOH, M., KUNO, H., YOSHIDA, T., KONDO, H. & TAKEUCHI, M. 1998. Platelet-like particle formation in the human megakaryoblastic leukaemia cell lines, MEG-01 and MEG-01s. *Br J Haematol,* 100**,** 436-44.

TOMURA, S., NAKAMURA, Y., DEGUCHI, F., ANDO, R., CHIDA, Y. &

MARUMO, F. 1991. Coagulation and fibrinolysis in patients with chronic renal failure undergoing conservative treatment. *Thromb Res,* 64**,** 81-90.

VARGA-SZABO, D., BRAUN, A., KLEINSCHNITZ, C., BENDER, M., PLEINES, I., PHAM, M., RENNE, T., STOLL, G. & NIESWANDT, B. 2008. The calcium sensor STIM1 is an essential mediator of arterial thrombosis and ischemic brain infarction. *J Exp Med,* 205**,** 1583-91.

VARGA-SZABO, D., BRAUN, A. & NIESWANDT, B. 2011. STIM and Orai in platelet function. *Cell Calcium,* 50**,** 270-8.

VARGHESE, A., LACSON, E., JR., SONTROP, J. M., ACEDILLO, R. R., AL-JAISHI, A. A., ANDERSON, S., BAGGA, A., BAIN, K. L., BENNETT, L. L., BOHM, C., BROWN, P. A., CHAN, C. T., COTE, B., DEV, V., FIELD, B., HARRIS, C., KALATHARAN, S., KIAII, M., MOLNAR, A. O., OLIVER, M. J., PARMAR, M. S., SCHORR, M., SHAH, N., SILVER, S. A., SMITH, D. M., SOOD, M. M., ST LOUIS, I., TENNANKORE, K. K., THOMPSON, S., TONELLI, M., VORSTER, H., WALDVOGEL, B., ZACHARIAS, J., GARG, A. X. & DIALYSATE MAGNESIUM, I. 2020. A Higher Concentration of Dialysate Magnesium to Reduce the Frequency of Muscle Cramps: A Narrative Review. *Can J Kidney Health Dis,* 7**,** 2054358120964078.

VORMANN, J. 2003. Magnesium: nutrition and metabolism. *Mol Aspects Med,* 24**,** 27-37.

WANG, J., XU, C., ZHENG, Q., YANG, K., LAI, N., WANG, T., TANG, H. & LU, W. 2017a. Orai1, 2, 3 and STIM1 promote store-operated calcium entry in pulmonary arterial smooth muscle cells. *Cell Death Discov,* 3**,** 17074.

WANG, Y., ZHAO, Z., SHI, S., GAO, F., WU, J., DONG, S., ZHANG, W., LIU, Y. & ZHONG, X. 2017b. Calcium sensing receptor initiating cystathionine-gamma-lyase/hydrogen sulfide pathway to inhibit platelet activation in hyperhomocysteinemia rat. *Exp Cell Res,* 358**,** 171-181.

WILLIAMS, R. T., MANJI, S. S., PARKER, N. J., HANCOCK, M. S., VAN STEKELENBURG, L., EID, J. P., SENIOR, P. V., KAZENWADEL, J. S., SHANDALA, T., SAINT, R., SMITH, P. J. & DZIADEK, M. A. 2001. Identification and characterization of the STIM (stromal interaction molecule) gene family: coding for a novel class of transmembrane proteins. *Biochem J,* 357**,** 673-85.

WOOLTHUIS, C. M. & PARK, C. Y. 2016. Hematopoietic stem/progenitor cell commitment to the megakaryocyte lineage. *Blood,* 127**,** 1242-8.

WU, H., LI, Q., FAN, L., ZENG, D., CHI, X., GUAN, B., HU, B., LU, Y., YUN, C., KRAMER, B., HOCHER, B., LIU, F. & YIN, L. 2021. Prognostic Value of Serum Magnesium in Mortality Risk among Patients on Hemodialysis: A Meta-Analysis of Observational Studies. *Kidney Dis (Basel),* 7**,** 24-33.

XIONG, J., HE, T., WANG, M., NIE, L., ZHANG, Y., WANG, Y., HUANG, Y.,

FENG, B., ZHANG, J. & ZHAO, J. 2019. Serum magnesium, mortality, and cardiovascular disease in chronic kidney disease and end-stage renal disease patients: a systematic review and meta-analysis. *J Nephrol,* 32**,** 791-802.

XU, P., LU, J., LI, Z., YU, X., CHEN, L. & XU, T. 2006. Aggregation of STIM1 underneath the plasma membrane induces clustering of Orai1. *Biochem Biophys Res Commun,* 350**,** 969-76.

YANG, K., DU, C., WANG, X., LI, F., XU, Y., WANG, S., CHEN, S., CHEN, F., SHEN, M., CHEN, M., HU, M., HE, T., SU, Y., WANG, J. & ZHAO, J. 2017. Indoxyl sulfate induces platelet hyperactivity and contributes to chronic kidney disease-associated thrombosis in mice. *Blood,* 129**,** 2667-2679.

YUAN, J. P., ZENG, W., DORWART, M. R., CHOI, Y. J., WORLEY, P. F. & MUALLEM, S. 2009. SOAR and the polybasic STIM1 domains gate and regulate Orai channels. *Nat Cell Biol,* 11**,** 337-43.

ZELT, J. G., MCCABE, K. M., SVAJGER, B., BARRON, H., LAVERTY, K., HOLDEN, R. M. & ADAMS, M. A. 2015. Magnesium Modifies the Impact of Calcitriol Treatment on Vascular Calcification in Experimental Chronic Kidney Disease. *J Pharmacol Exp Ther,* 355**,** 451-62.

ZHANG, C., ZHANG, T., ZOU, J., MILLER, C. L., GORKHALI, R., YANG, J. Y., SCHILMILLER, A., WANG, S., HUANG, K., BROWN, E. M., MOREMEN, K. W., HU, J. & YANG, J. J. 2016. Structural basis for regulation of human calcium-sensing receptor by magnesium ions and an unexpected tryptophan derivative co-agonist. *Sci Adv,* 2**,** e1600241.

ZHANG, L., CUI, R., CHENG, X. & DU, J. 2005a. Antiapoptotic effect of serum and glucocorticoid-inducible protein kinase is mediated by novel mechanism activating I{kappa}B kinase. *Cancer Res,* 65**,** 457-64.

ZHANG, S. L., YU, Y., ROOS, J., KOZAK, J. A., DEERINCK, T. J., ELLISMAN, M. H., STAUDERMAN, K. A. & CAHALAN, M. D. 2005b. STIM1 is a Ca2+ sensor that activates CRAC channels and migrates from the Ca2+ store to the plasma membrane. *Nature,* 437**,** 902-5.

ZHANG, W., SUN, R., ZHONG, H., TANG, N., LIU, Y., ZHAO, Y., ZHANG, T. & HE, F. 2019. CaSR participates in the regulation of vascular tension in the mesentery of hypertensive rats via the PLCIP3/ACV/cAMP/RAS pathway. *Mol Med Rep,* 20**,** 4433-4448.

ZHENG, L., STATHOPULOS, P. B., SCHINDL, R., LI, G. Y., ROMANIN, C. & IKURA, M. 2011. Auto-inhibitory role of the EF-SAM domain of STIM proteins in store-operated calcium entry. *Proc Natl Acad Sci U S A,* 108**,** 1337-42.

ZHOU, K., ZHU, X., MA, K., LIU, J., NURNBERG, B., GAWAZ, M. & LANG, F. 2021. Effect of MgCl2 and GdCl3 on ORAI1 Expression and Store-

Operated Ca(2+) Entry in Megakaryocytes. *Int J Mol Sci,* 22.

ZHOU, Y., MANCARELLA, S., WANG, Y., YUE, C., RITCHIE, M., GILL, D. L. & SOBOLOFF, J. 2009. The short N-terminal domains of STIM1 and STIM2 control the activation kinetics of Orai1 channels. *J Biol Chem,* 284**,** 19164-8.

ZHOU, Y., SRINIVASAN, P., RAZAVI, S., SEYMOUR, S., MERANER, P., GUDLUR, A., STATHOPULOS, P. B., IKURA, M., RAO, A. & HOGAN, P. G. 2013. Initial activation of STIM1, the regulator of store-operated calcium entry. *Nat Struct Mol Biol,* 20**,** 973-81.

ZHU, X., MA, K., ZHOU, K., VOELKL, J., ALESUTAN, I., LEIBROCK, C., NURNBERG, B. & LANG, F. 2020. Reversal of phosphate-induced ORAI1 expression, store-operated Ca(2+) entry and osteogenic signaling by MgCl2 in human aortic smooth muscle cells. *Biochem Biophys Res Commun,* 523**,** 18-24.

8 Declaration of contributions

This work was conducted in the Department of Pharmacology, Experimental Therapy & Toxicology at the Eberhard Karls Universty Tübingen under the supervision of Prof. Dr. Dr. Florian Lang and Prof. Dr. Dr. Bernd Nürnberg.

Prof. Dr. Dr. Florian Lang, Prof. Dr. Dr. Bernd Nürnberg and Prof. Dr. Meinrad Gawaz were responsible for the design the conception of this study. I performed all of the experiments and analyzed all the data. In addition, the completion of this project has benefited from Ke Ma and Xuexue Zhu for their kind help in experimental techniques, and Jibin Liu for his help in data analysis.

I hereby declare that this submitted dissertation entitled: "Effects of $MgCl_2$ and $GdCl_3$ on ORAI1 Expression and Store-Operated Ca^{2+} Entry in Megakaryocytes" was written by myself independently. All the figures presented in the results section was prepared by myself.

9 Publication

Parts of the present work (data in figure 5, 7-9, 11-14) were published in the following paper:

Title:

Effect of $MgCl_2$ and $GdCl_3$ on ORAI1 Expression and Store-Operated Ca^{2+} Entry in Megakaryocytes.

Author:

Zhou K, Zhu X, Ma K, Liu J, Nürnberg B, Gawaz M, Lang F.

Journal:

International Journal of Molecular Sciences. 2021,22(7):3292.

10 Acknowledgements

the nice figure and hope we can meet up again someday in the future.

Last, but by no means least, I would like to thank my family members who are far away from me but keep their love and support no matter of distances. Their endless support and engouement is always the source of my confidence and give me strength to move forward.